

Co-clustering of Spatially Resolved Transcriptomic Data

A. Sottosanti¹ and D. Risso¹

¹University of Padova, Department of Statistical Sciences,

via Cesare Battisti 241-243, Padova, Italy

October 12, 2021

Address for correspondence: andrea.sottosanti@unipd.it

Abstract

Spatial transcriptomics is a modern sequencing technology that allows the measurement of the activity of thousands of genes in a tissue sample and map where the activity is occurring. This technology has enabled the study of the so-called spatially expressed genes, i.e., genes which exhibit spatial variation across the tissue. Comprehending their functions and their interactions in different areas of the tissue is of great scientific interest, as it might lead to a deeper understanding of several key biological mechanisms. However, adequate statistical tools that exploit the newly spatial mapping information to reach more specific conclusions are still lacking.

In this work, we introduce SPARTACO, a new statistical model that clusters the spatial expression profiles of the genes according to the areas of the tissue. This is accomplished by performing a co-clustering, i.e., inferring the latent block structure of the data and inducing two types of clustering: of the genes, using their expression across the tissue, and of the image areas, using the gene expression in the spots where the RNA is collected. Our proposed methodology is validated with a series of simulation experiments and its usefulness in responding to specific biological questions is illustrated with an application to a human brain tissue sample processed with the 10X-Visium protocol.

Keywords: Co-clustering; EM algorithm; Genomics; Integrated complete log-likelihood; Human dorsolateral pre-frontal cortex; Model based clustering; Spatial transcriptomics, 10X-Visium.

1 Introduction

1.1 The rise of spatial transcriptomics

In the last few years, we have witnessed a dramatic improvement in the efficiency of DNA sequencing technologies that ultimately gave rise to new advanced protocols for single-cell RNA sequencing (scRNA-seq) and, more recently, spatial transcriptomics. With respect to scRNA-seq, spatial transcriptomics platforms are able to provide, in addition to the abundance, the locations of thousands of genes in a tissue sample.

Righelli *and others* (2021) classify spatial transcriptomic protocols into *molecule-based* and *spot-based* methods. Among molecule-based methods, seqFISH (Lubeck *and others*, 2014) is one of the more established protocols and is capable of providing the spatial expression of thousands of transcripts at a sub-cellular level. Similar methods include MERFISH (Chen *and others*, 2015), Slide-seq (Rodrigues *and others*, 2019) and ZipSeq (Hu *and others*, 2020). Molecule-based methods offer a higher resolution than spot-based protocols, but the setup necessary to reproduce these kinds of spatial experiments is often complex and expensive to recreate.

The new *Visium* platform from 10X-Genomics (Rao *and others*, 2020) has brought the use of transcriptomic experiments to a new level, providing a technology that allows scientists to achieve a full mapping of the cellular structure of a tissue sample in a relatively easy manner. Visium, as all the other *spot-based* methods, has a substantially lower resolution than molecular-based methods; however, in addition to being more sensitive, it is widely and easily accessible to the scientific community (Zhao *and others*, 2021). The data collecting process is performed by placing a slice of the tissue of interest over a grid of spots, so that every spot contains few neighbor cells. The gene expression of each spot is then characterized, resulting in a dataset made of tens of thousands of genes for each spot, together with the spatial location of the spots. Figure 1 shows an example of human dorsolateral pre-frontal cortex (DLPFC) processed with Visium at the Lieber Institute for Brain Development (Maynard *and others*, 2021). The colored dots denote a manual annotation of the spots performed by Maynard *and others* (2021). The dataset is available in the R package **spatialLIBD** (Pardo *and others*, 2021).

The rise of spatial transcriptomics has motivated the development of new statistical methods that handle the identification of *spatially expressed* (s.e.) genes, i.e., genes with spatial patterns of expression variation across the tissue. Specific inferential procedures for detecting such kind of genes, such as SpatialDE (Svensson *and others*, 2018) and Trendsseek (Edsgård *and others*, 2018), have been proposed only in the last years. These methods are widely computationally efficient, but sometimes they reach discordant inferential conclusions, and additionally they fail to account for the correlation of the genes. The very recent algorithm by Sun *and others* (2020), called SPARK, has addressed some of the limitations of the earlier methods. However, the additional information brought by

the new spatial transcriptomic platforms has raised several questions, both on the biological and statistical side: detecting the s.e. genes is thus not the end of the analysis but just its beginning. In this article, we want to focus on three specific research questions, i.e., to determine:

- i.) the clustering of the areas of the tissue sample exploiting the additional spatial information brought by the spatial transcriptomic platforms;
- ii.) the existence of clusters of genes which are s.e. only in some of the areas discovered from i.);
- iii.) the highly variable genes in the areas discovered from i.) net of any spatial effect.

Research question i.) is fundamental for the analysis of tissue samples because it is the starting point for successive downstream analyses. The recent GIOTTO (Dries *and others*, 2021) and BayesSpace (Zhao *and others*, 2021) methods are unsupervised clustering algorithms designed for spot-based spatial transcriptomics, developed on the principle that neighboring spots are likely to be annotated with the same label.

Research question ii.) is of great scientific interest, but, to the best of our knowledge, has not been tackled yet. Discovering that some genes are s.e. only in some areas of the tissue would play a core role in comprehending some fundamental biological mechanisms, and ultimately discovering new ones. Even the very recent SPARK method for detecting s.e. genes is not designed to state if the spatial expression activity of a gene is restricted to specific areas of the tissue. With the existing statistical tools, one can approach this issue with a two-step analysis, first clustering the image using BayesSpace or GIOTTO, and then applying SPARK to each of the discovered clusters. However, such heuristic procedure has some limitations. First, repeating the tests in each of the image cluster requires to control for multiple testing, e.g., by controlling the False Discovery Rate (Benjamini and Hochberg, 1995). Second, even after the s.e. genes are isolated, an additional clustering of the genes is necessary to perform specific downstream analyses (Svensson *and others*, 2018; Sun *and others*, 2020). Last, if indeed there are clusters of genes, such information should be accounted for in the first step of the procedure, when the image is clustered.

Finally, research question iii.) has the goal of determining which genes are active in each of the image cluster. Thanks to the spatial mapping of the spots, it will be possible to separate the presence of spatial effects from the total variation of each gene, providing a more accurate list of highly variable genes.

1.2 A co-clustering perspective

In this article, we consider the problem of modelling and clustering gene expression in a tissue sample processed with a spot-based spatial transcriptomic method, such as 10X

Visium, and measured over a set of spatially located sites.

In the remainder of the article, we use “spots” to denote the spots in the tissue from which RNA is extracted and “genes” to denote the variables measured in each spot, using a terminology typical of the Visium platform. However, the method presented here is more general and can be applied to any spatial transcriptomic technology and, more broadly, to any dataset for which the rows or the columns are measured in some observational sites with known coordinates.

We tackle the research questions outlined above as a single, two-directional clustering problem: of the genes, using spots as variables, and of the spots, using genes as variables. This kind of procedure is known in the literature as *co-clustering* (or *block-clustering*, Bouveyron *and others*, 2019) and denotes the act of clustering both the rows and the columns of a data matrix, which, in this way, is partitioned into rectangular, non-overlapping sub-matrices called *co-clusters* (or *blocks*).

Bouveyron *and others* (2019) distinguish between *deterministic* and *model-based* co-clustering approaches. Model-based methods are designed to simultaneously perform the clustering and reconstruct the probabilistic generative mechanism of the data. The model-based co-clustering literature is centered around the Latent Block Model (LBM; Govaert and Nadif, 2013), an extension of the standard mixture modelling approach when both rows and columns of a data matrix are deemed to come from some underlying clusters. Thanks to the ease of interpretation and to the raise of new advanced computational methods, the LBM has been extensively explored as a tool for modelling continuous (Govaert and Nadif, 2013, Chapter 5), categorical (Keribin *and others*, 2015), count (Govaert and Nadif, 2010), binary (Govaert and Nadif, 2008) and recently even functional data (Bouveyron *and others*, 2017; Casa *and others*, 2021). In addition, both frequentist (Govaert and Nadif, 2008; Bouveyron *and others*, 2017) and Bayesian (Wyse and Friel, 2012; Keribin *and others*, 2015) approaches have been proposed for fitting these models. The conditional independence assumption of LBM states that the observations within the same co-cluster are independent. Surely, this hypothesis is computationally attractive, yet it is incompatible with the high correlation levels shown by gene expression data (Efron, 2009). Tan and Witten (2014) overcome the conditional independence assumption proposing a co-clustering model based on the matrix variate Gaussian distribution (Gupta and Nagar, 2018), which accounts for the dependency across the rows and the columns in a block with two non-diagonal covariance matrices. Their model represents a first attempt to extend k-means-type algorithms for co-clustering to the case where the data entries in a block are not independent. The estimation of the needed covariance matrices is challenging; a challenge that can be overcome with the aid of a penalization term, such as the LASSO (Tibshirani, 1996; Witten and Tibshirani, 2009), to avoid singularity problems. However, with spatial data, it is natural to leverage the spatial dependencies observed in the data to aid the covariance matrix estimation.

Here, we propose SPARTACo (SPAtially Resolved TrAnscriptomics CO-clustering), a novel co-clustering technique designed for discovering the hidden block structure of spatial transcriptomic data. Since the spots in which gene expression is measured are spatially located on a grid, our model expresses the correlation across transcripts in different spots as a function of their distances. As a consequence, differently from the rest of the co-clustering models proposed in the literature, SPARTACo divides the data matrix into blocks based on the estimated means, variances, and spatial covariances. In addition, we use gene-specific random effects to account for the remaining covariance not explained by the spatial structure.

Although the published literature is not always clear about the distinction between *co-clustering* and *biclustering*, in accordance with the recent works of Moran *and others* (2021) and Murua and Quintana (2021) here we adopt the following terminology: both co-clustering and biclustering are families of techniques used to group the rows and the columns of a data matrix. However, in biclustering the groups formed, called *biclusters*, can take any possible shape, while co-clustering is limited to rectangular, non-overlapping blocks. In addition, biclustering algorithms do not necessarily allocate all the data entries into one of the existent biclusters, and so some entries can be left unassigned. Although biclustering methods are more flexible, the main advantage of co-clustering is that the returned blocks are often easier to interpret both from a statistical and practical perspective.

1.3 Outline

The rest of the manuscript is structured as follows. Section 2 illustrates the SPARTACo modelling approach and reviews some competing co-clustering models, highlighting the similarities and the differences with our proposal. Section 3 discusses some identifiability issues, illustrates our classification-stochastic EM (CS-EM) algorithm for parameter estimation, and derives a model selection criterion based on the *integrated complete log-likelihood* (Biernacki *and others*, 2000). Section 4 proposes five simulated spatial experiments of growing complexity with whom we compare SPARTACo with other co-clustering models. Section 5 shows how our proposal allows to answer our three research questions using a region of a tissue sample from the human brain. The manuscript is concluded by some considerations of the possible future extensions.

2 The statistical model

Let $\mathbf{X} = (x_{ij})_{1 \leq i \leq n, 1 \leq j \leq p}$ be the $n \times p$ matrix of a spatial experiment processed by a spot-based spatial transcriptomic platform, i.e, containing the expression of n genes over a grid of p spots on the chip surface. The spatial location of the spot j over the chip

surface is known through its spatial coordinates $\mathbf{s}_j = (s_{jx}, s_{jy})$; we name as $\mathbf{S} = (\mathbf{s}_j)_{1 \leq j \leq p}$ the $p \times 2$ matrix containing the coordinates of the p spots. From this point, we assume that the data entries in \mathbf{X} have been properly pre-processed, and so $x_{ij} \in \mathbb{R}$ for any i and j .

2.1 Model formulation

We assume there exist K clusters of rows of \mathbf{X} , and R clusters of columns of \mathbf{X} , forming a latent structure of KR blocks. The vectors of random variables $\mathcal{Z} = (\mathcal{Z}_i)_{1 \leq i \leq n}$ and $\mathcal{W} = (\mathcal{W}_j)_{1 \leq j \leq p}$ denote to which cluster the rows and the columns belong, respectively. Thus, $\mathcal{C}_k = \{i = 1, \dots, n : \mathcal{Z}_i = k\}$ is the k -th row cluster, with $k = 1, \dots, K$, and $\mathcal{D}_r = \{j = 1, \dots, p : \mathcal{W}_j = r\}$ is the r -th column cluster, with $r = 1, \dots, R$. The cluster dimensions are $n_k = |\mathcal{C}_k|$ and $p_r = |\mathcal{D}_r|$. The notation used to refer to subsets of \mathbf{X} is the following: $\mathbf{X}^{kr} = (x_{ij})_{i \in \mathcal{C}_k, j \in \mathcal{D}_r}$ is the kr -th co-cluster (block), $\mathbf{X}^{k\cdot} = (x_{ij})_{i \in \mathcal{C}_k, 1 \leq j \leq p}$ is the $n_k \times p$ matrix formed by all the rows in \mathcal{C}_k , and $\mathbf{X}^{\cdot r} = (x_{ij})_{1 \leq i \leq n, j \in \mathcal{D}_r}$ is the $n \times p_r$ matrix formed by all the columns in \mathcal{D}_r . When it comes to access the elements of a block, we use the notation $\mathbf{X}^{kr} = (x_{ij}^{kr})_{1 \leq i \leq n_k, 1 \leq j \leq p_r}$. So, the i -th row vector and the j -th column vector of \mathbf{X}^{kr} are respectively $\mathbf{x}_i^{kr} = (x_{ij}^{kr})_{1 \leq j \leq p_r}$ and $\mathbf{x}_j^{kr} = (x_{ij}^{kr})_{1 \leq i \leq n_k}$.

The vector \mathbf{x}_i^{kr} contains the expression of the i -th gene in the cluster \mathcal{C}_k across the p_r spots in the cluster \mathcal{D}_r . We model \mathbf{x}_i^{kr} as

$$\mathbf{x}_i^{kr} = \mu_{kr} \mathbf{1}_{p_r} + \sigma_{kr,i} \boldsymbol{\epsilon}_i^{kr}, \quad \boldsymbol{\epsilon}_i^{kr} \sim \mathcal{N}_{p_r}(\mathbf{0}, \boldsymbol{\Delta}_{kr}), \quad (1)$$

$$\boldsymbol{\Delta}_{kr} = \tau_{kr} \mathcal{K}(\mathbf{S}^r; \boldsymbol{\phi}_r) + \xi_{kr} \mathbb{I}_{p_r}, \quad (2)$$

where μ_{kr} is a scalar mean parameter, $\mathbf{1}_{p_r}$ is a vector of ones, $\sigma_{kr,i}^2$ is a gene-specific variance, and $\boldsymbol{\Delta}_{kr}$ is the covariance matrix of the columns. Following Svensson *and others* (2018) and Sun *and others* (2020), Formula (2) expresses $\boldsymbol{\Delta}_{kr}$ as a linear combination of two matrix terms: \mathbb{I}_{p_r} is a diagonal matrix of order p_r , $\mathcal{K}(\mathbf{S}^r; \boldsymbol{\phi}_r) = (k(\|\mathbf{s}_j^r - \mathbf{s}_{j'}^r\|; \boldsymbol{\phi}_r))_{1 \leq j, j' \leq p_r}$ is the spatial covariance matrix, where $k(\cdot; \boldsymbol{\phi}_r)$ is an *isotropic* spatial covariance function (Gaetan and Guyon, 2010, Section 1.2) parametrized by a vector $\boldsymbol{\phi}_r$, and $\mathbf{S}^r = (\mathbf{s}_j)_{j \in \mathcal{D}_r}$ is the sub-matrix of \mathbf{S} containing the spots in \mathcal{D}_r . The term *isotropic* denotes that the covariance between two points $j, j' \in \mathcal{D}_r$ depends just on the distance between their two sites, $\|\mathbf{s}_j^r - \mathbf{s}_{j'}^r\|$. The positive parameters τ_{kr} and ξ_{kr} in Formula (2) handle the linear combination between \mathcal{K} and \mathbb{I}_{p_r} : the former measures the spatial dependence of the data, the latter is the so-called *nugget effect*, a residual variance.

According to Section 2.4 of Cressie (2015), to select an adequate spatial covariance kernel for the data, one can explore the empirical spatial dependency through the *variogram* and then select a kernel from a vast list of proposals (see for example Rasmussen and Williams, 2006 and Gaetan and Guyon, 2010). However, under our model, this strategy would be unfeasible because only the data within the same cluster are spatially dependent,

so the selection of the spatial covariance kernel should be performed simultaneously with the clustering of the data. As a compromise, SPARTACo considers the same covariance model $k(\cdot; \boldsymbol{\phi}_r)$ for every column cluster \mathcal{D}_r ; the only difference among the kernels of the clusters is the value of the model parameters $\boldsymbol{\phi}_r$.

The scale parameters $\sigma_{kr,i}^2$ in (1) aim to capture the variability left unexplained by the spatial covariance model (2), and eventually a possible extra source of variability of the data that might be due to the dependency across genes. In the longitudinal data framework, De la Cruz-Mesía and Marshall (2006) and Anderlucci and Viroli (2015) consider a random effect model to account for the systematic dependency across subjects in the same group of study. We follow the same approach and we assume that every $\sigma_{kr,i}^2$ is a realization of an Inverse Gamma distribution $\mathcal{IG}(\alpha_{kr}, \beta_{kr})$, where α_{kr} and β_{kr} denote the shape and the rate, respectively. The Inverse Gamma is chosen for its conjugacy with the Gaussian distribution and allows to derive the marginal probability density of \mathbf{x}_i^{kr} , that is

$$f(\mathbf{x}_i^{kr}; \boldsymbol{\theta}_{kr}, \boldsymbol{\phi}_r) = \frac{1}{\sqrt{2\pi|\boldsymbol{\Delta}_{kr}|}} \frac{\Gamma(\alpha_{kr}^*)}{\Gamma(\alpha_{kr})} \frac{\beta_{kr}^{\alpha_{kr}}}{\beta_{kr,i}^* \alpha_{kr,i}^*}, \quad (3)$$

where $|\cdot|$ denotes the matrix determinant, $\alpha_{kr,i}^* = p_r/2 + \alpha_{kr}$ and $\beta_{kr,i}^* = (\mathbf{x}_i^{kr} - \mu_{kr} \mathbf{1}_{p_r})^T \boldsymbol{\Delta}_{kr}^{-1} (\mathbf{x}_i^{kr} - \mu_{kr} \mathbf{1}_{p_r})/2 + \beta_{kr}$. The set of parameters $\boldsymbol{\theta}_{kr} = \{\mu_{kr}, \tau_{kr}, \xi_{kr}, \alpha_{kr}, \beta_{kr}\}$ is specific of the data into the (k, r) -th co-cluster, while $\boldsymbol{\phi}_r$ is a parameter that is descriptive of the entire r -th column cluster. Note that this formulation is similar to that employed to *shrink* the gene variances in the popular *Limma* model (Smyth, 2004).

The model in Formula (1) can be rephrased with a probability distribution over the entire kr -th block, $\mathbf{X}^{kr} | \boldsymbol{\Sigma}_{kr} \sim \mathcal{MVN}(\mu_{kr} \mathbf{1}_{n_k \times p_r}, \boldsymbol{\Sigma}_{kr}, \boldsymbol{\Delta}_{kr})$, where \mathcal{MVN} denotes the matrix-variate normal distribution and $\boldsymbol{\Sigma}_{kr} = \text{diag}(\sigma_{kr,1}^2, \dots, \sigma_{kr,n_k}^2)$ is the (diagonal) covariance matrix of the genes. A consequence of the matrix-variate normal model is that every row, column and sub-matrix of \mathbf{X}^{kr} is Gaussian (Gupta and Nagar, 2018). For instance, the following model formulation is equivalent to Formula (1):

$$\mathbf{x}_{\cdot j}^{kr} | \boldsymbol{\Sigma}_{kr} \sim \mathcal{N}_{n_k} \{ \mu_{kr} \mathbf{1}_{n_k}, (\tau_{kr} + \xi_{kr}) \boldsymbol{\Sigma}_{kr} \}, \quad \text{Cov}(\mathbf{x}_{\cdot j}^{kr}, \mathbf{x}_{\cdot j'}^{kr}) = \tau_{kr} k (||\mathbf{s}_j^r - \mathbf{s}_{j'}^r||; \boldsymbol{\phi}_r) \boldsymbol{\Sigma}_{kr},$$

with $j, j' \in \mathcal{D}_r$.

Last, the clustering labels \mathcal{Z} and \mathcal{W} are unknown independent random variables. Figure 2 represents the relations across the elements of the model with a DAG.

2.2 A comparison with other co-clustering models

We review in this section some advanced co-clustering techniques which have some similarities with our proposal. The goal is to highlight, starting from the existing literature, how SPARTACo has been designed specifically for detecting and clustering data based on their spatial covariance in some groups of observational sites.

With respect to the distinction between deterministic and model-based co-clustering techniques we already discussed in Section 1.2, we choose to compare SPARTACo only with model-based techniques because they offer a clear advantage in the interpretation of the results. Some of the methods that we review here are named as biclustering models, but in practice they segment the data matrix into rectangular blocks.

- *Sparse Biclustering* (PARSEBC, Tan and Witten, 2014) extends the k -means algorithm to the co-clustering framework. The model corresponds to a probabilistic assumption on the block of the type $\mathbf{X}^{kr} \sim \mathcal{MVN}(\mu_{kr} \mathbf{1}_{n_k \times p_r}, \mathbb{I}_{n_k}, \xi \mathbb{I}_{p_r})$, where ξ is an unknown scale parameter. In PARSEBC, the estimation of μ_{kr} , for any k and r , is regulated by a LASSO penalization. We thus distinguish the sparse estimation from the case of null penalization (BC).
- *Matrix-Variate Normal Biclustering* (MVNB, Tan and Witten, 2014) extends PARSEBC by taking a probabilistic model on the blocks of the type $\mathbf{X}^{kr} \sim \mathcal{MVN}(\mu_{kr} \mathbf{1}_{n_k \times p_r}, \boldsymbol{\Sigma}_k^{\text{MVNB}}, \boldsymbol{\Delta}_r^{\text{MVNB}})$, where both $\boldsymbol{\Sigma}_k^{\text{MVNB}}$ and $\boldsymbol{\Delta}_r^{\text{MVNB}}$ are non-diagonal covariance matrices with respectively $n_k(n_k + 1)/2$ and $p_r(p_r + 1)/2$ free parameters. Together with the LASSO penalization on the centroids, handled by a parameter λ , the authors deploy a graphical LASSO penalization (Witten and Tibshirani, 2009) to practically solve the singularity problems in the estimate of $\boldsymbol{\Sigma}_k^{\text{MVNB}}$ and $\boldsymbol{\Delta}_r^{\text{MVNB}}$. The penalization parameters involved are denoted by $\rho_{\boldsymbol{\Sigma}}$ and $\rho_{\boldsymbol{\Delta}}$.

With respect to the MVNB, SPARTACo has specific row and column covariance matrices $\boldsymbol{\Sigma}_{kr}$ and $\boldsymbol{\Delta}_{kr}$ for each block, whose structure is described in Section 2.1. The total number of free parameter, $KR|\boldsymbol{\theta}_{kr}| + R|\boldsymbol{\phi}_r|$, does not grow either with n or p . As a direct consequence, the parameter estimation of SPARTACo, conditioning on the clustering labels \mathcal{Z} and \mathcal{W} , remains much less computationally prohibitive than the one of the MVNB, specially when the sample size becomes considerably large.

- *Latent Block Model* is a vast class of statistical models that can be seen as an extension of the mixture model for co-clustering problems. The model for continuous data (Govaert and Nadif, 2013, Chapter 5) can be written using the Matrix Variate Normal representation as $\mathbf{X}^{kr} \sim \mathcal{MVN}(\mu_{kr} \mathbf{1}_{n_k \times p_r}, \mathbb{I}_{n_k}, \xi_{kr} \mathbb{I}_{p_r})$ and so it is based on the assumption that the data entries in a block are independent given the clustering labels (conditional independence). The intra-block model is thus a special case of SPARTACo when $\boldsymbol{\Sigma}_{kr} = \mathbb{I}$ and $\tau_{kr} = 0$, for all k and r . However, the LBM is more general on the probabilistic assumptions over the clustering variables. In fact, it assumes $\Pr(\mathcal{Z}_i = k) = \pi_k$ and $\Pr(\mathcal{W}_j = r) = \rho_r$, where (π_1, \dots, π_K) and (ρ_1, \dots, ρ_R) are probability vectors such that $\sum_{k=1}^K \pi_k = \sum_{r=1}^R \rho_r = 1$, while

SPARTACo implicitly assumes that $\Pr(\mathcal{Z}_i = k) = 1/K$ and $\Pr(\mathcal{W}_i = k) = 1/R$ for any k and r .

Supplementary Figure 2 gives a summary of the relations across SPARTACo and the co-clustering models discussed in this section.

3 Inference

3.1 Identifiability

The model as expressed in Formula (1) is not identifiable in the covariance term: in fact, for any $a > 0$, $\sigma_{kr,i}^2 \cdot \Delta_{kr} = a\sigma_{kr,i}^2 / a = \tilde{\sigma}_{kr,i}^2 \cdot \tilde{\Delta}_{kr}$. This issue generates in practice an infinite number of solutions for the parameter estimate.

A typical workaround to get unique parameter estimates consists in setting the value of some covariance parameters. In our model, this would mean taking $\sigma_{kr,i}^2 = c$, for one i in $\{1, \dots, n_k\}$, using an arbitrary positive constant c . Incidentally, this is equivalent to constraint $\text{tr}(\Sigma_{kr})$, the trace of the matrix Σ_{kr} (Allen and Tibshirani, 2010; Caponera and others, 2017). However, we discard this solution as, under our model, the rows of the data matrix are involved into a clustering procedure. Thus, it is not possible to define which i in a cluster should take the constraint.

The solution we adopt for our model puts the identification constraint on Δ_{kr} (Anderlucci and Viroli, 2015). Since $\text{tr}(\Delta_{kr}) = p_r(\tau_{kr} + \xi_{kr})$, we constraint the quantity $\tau_{kr} + \xi_{kr} = c_\Delta$, where c_Δ is an arbitrary positive constant. Such constraint has a notable practical consequence: in fact, once the estimate $\hat{\tau}_{kr}$ is determined within the constrained domain $(0, c_\Delta)$, then $\hat{\xi}_{kr}$ is simply taken by difference as $\hat{\xi}_{kr} = c_\Delta - \hat{\tau}_{kr}$. Hence, we can only interpret $\hat{\tau}_{kr}$ and $\hat{\xi}_{kr}$ in relation to each other and not in absolute terms. According to Svensson and others (2018), in our applications (Sections 4 and 5) we will consider the quantity τ_{kr}/ξ_{kr} that we called *spatial signal-to-noise ratio*. This ratio is easily interpretable because it represents the amount of spatial expression of the genes in a cluster with respect to the nugget effect.

3.2 Model estimation

To estimate SPARTACo, we propose an approach based on the maximization of the *classification log-likelihood*, that is

$$\log \mathcal{L}(\boldsymbol{\Theta}, \mathcal{Z}, \mathcal{W}) = \sum_{i=1}^n \sum_{k=1}^K \mathbb{1}(\mathcal{Z}_i = k) \left\{ \sum_{r=1}^R \log f(\mathbf{x}_i^r; \boldsymbol{\theta}_{kr}, \boldsymbol{\phi}_r) \right\}, \quad (4)$$

where \mathbf{x}_i^r is the i -th row of the matrix \mathbf{X}^r and $f(\cdot; \cdot)$ is given in Formula (3). Notice that the correlation across the columns does not allow to write the \mathbf{W} explicitly. This issue does not concern the \mathbf{Z} , because the rows are independent.

Chapter 2 of Bouveyron *and others* (2019) makes a clear distinction between the classification and the *complete log-likelihood* (the latter includes an additional part related to the distribution of the clustering labels). However, since SPARTACo implicitly assumes that $\Pr(\mathcal{Z}_i = k) = 1/K$ and $\Pr(\mathcal{W}_i = k) = 1/R$ for any k and r , then there is no practical difference between classification and complete log-likelihood.

The classification log-likelihood can be maximized with a *classification EM* algorithm (CEM, Celeux and Govaert, 1992), a modification of the standard EM which allocates the observations into the clusters during the estimation procedure. The CEM is an iterative algorithm which alternates between a classification step (CE Step), where the estimates of \mathbf{Z} and \mathbf{W} are updated, and a maximization step (M Step), which updates the parameter estimates of Θ . The benefits brought by such algorithm are particularly visible when complex models as the LBM are employed, because the joint conditional distribution $p(\mathbf{Z}, \mathbf{W} | \mathbf{X}; \Theta)$ is not directly available (Govaert and Nadif, 2013).

Under SPARTACo, a direct update of \mathbf{W} through a CE step is unfeasible due to the correlation across the columns, and so the estimation algorithm requires some modifications. This issue was already discussed by Tan and Witten (2014) for their MVNB model; however, their solution consists in an heuristic estimation algorithm with no guarantees of convergence. Since a classification step is unfeasible, we perform a stochastic allocation (SE step), where the column clustering configuration \mathbf{W} is sampled from a Markov chain whose limit distribution is the conditional distribution $p(\mathbf{W} | \mathbf{Z}, \mathbf{X}; \Theta)$. This step can be performed using the Metropolis-Hastings algorithm. A stochastic version of the EM algorithm was previously employed also for estimating the LBM by Keribin *and others* (2015), Bouveyron *and others* (2017) and Casa *and others* (2021).

Because of the alternation of a classification move, a stochastic allocation move and a maximization move, we name our algorithm *classification-stochastic EM* (CS-EM). We denote with $(\Theta, \mathbf{Z}, \mathbf{W})^{(t-1)}$ the estimate of the model parameters and of the clustering labels at iteration $t - 1$. At step t , the algorithm executes the following steps:

- **CE Step:** keeping fixed $(\mathbf{W}, \Theta)^{(t-1)}$, update the row clustering labels with the following rule:

$$\mathcal{Z}_i^{(t)} = \arg \max_{k=1, \dots, K} \frac{\prod_{r=1}^R f\left(\mathbf{x}_{i \cdot}^r; \boldsymbol{\theta}_{kr}^{(t-1)}, \boldsymbol{\phi}_r^{(t-1)}\right)}{\sum_{k'=1}^K \left\{ \prod_{r=1}^R f\left(\mathbf{x}_{i \cdot}^r; \boldsymbol{\theta}_{k'r}^{(t-1)}, \boldsymbol{\phi}_r^{(t-1)}\right) \right\}}, \quad i = 1, \dots, n.$$

- **SE Step:** keeping fixed $\mathbf{Z}^{(t)}$ and $\Theta^{(t-1)}$, the algorithm generates a candidate clustering configuration \mathbf{W}^* by randomly changing some elements from the starting

configuration $\mathcal{W}^{(t-1)}$. Let m be the number of elements of $\mathcal{W}^{(t-1)}$ that we attempt to change: m can be either fixed or randomly drawn from a discrete uniform distribution. To formulate \mathcal{W}^* , we exploit two moves.

(M1) Two clustering labels $g_1 \sim \mathcal{U}(\{1, \dots, R\})$ and $g_2 \sim \mathcal{U}(\{1, \dots, R\} \setminus \{g_1\})$ are drawn. The candidate configuration \mathcal{W}^* is made by selecting m observations from $\mathcal{W}^{(t-1)}$ at random with label g_1 and changing their label to g_2 . The quantity

$$\frac{q(\mathcal{W}^{(t-1)} | \mathcal{W}^*)}{q(\mathcal{W}^* | \mathcal{W}^{(t-1)})} = \frac{p_{g_1}! p_{g_2}!}{(p_{g_1} - m)! (p_{g_2} + m)!}$$

is the ratio of transition probabilities employed by the Metropolis-Hastings algorithm to evaluate \mathcal{W}^* , where $q(\mathcal{W}^* | \mathcal{W}^{(t-1)})$ and $q(\mathcal{W}^{(t-1)} | \mathcal{W}^*)$ are respectively the probabilities of passing from configuration $\mathcal{W}^{(t-1)}$ to \mathcal{W}^* and *vice-versa*. This move almost coincides with the (M2) move of Nobile and Fearnside (2007).

(M2) For $h = 1, \dots, m$, the clustering labels $g_{1h} \sim \mathcal{U}(\{1, \dots, R\})$ and $g_{2h} \sim \mathcal{U}(\{1, \dots, R\} \setminus \{g_{1h}\})$ are drawn. Let $b_{lr} = \sum_{h=1}^m \mathbf{1}(g_{lh} = r)$, for $l = 1, 2$ and $r = 1, \dots, R$. Then the candidate configuration \mathcal{W}^* is made by changing the labels of b_{1r} observations selected at random from the group r , when $b_{1r} > 0$, to $g_{2\kappa(r)}$, where $\kappa(r) = \{h = 1, \dots, m : g_{1h} = r\}$. The ratio of transition probabilities is

$$\frac{q(\mathcal{W}^{(t-1)} | \mathcal{W}^*)}{q(\mathcal{W}^* | \mathcal{W}^{(t-1)})} = \prod_{r: b_{2r} > 0} \frac{b_{2r}! (p_r - b_{1r})!}{(p_r - b_{1r} + b_{2r})!} \Big/ \prod_{r: b_{1r} > 0} \frac{b_{1r}! (p_r - b_{1r})!}{p_r!}.$$

The choice between (M1) and (M2) is random. The candidate configuration \mathcal{W}^* is accepted with probability $\min\{1, A\}$, where A is the following Metropolis-Hastings ratio:

$$A = \frac{\mathcal{L}(\boldsymbol{\Theta}^{(t-1)}, \mathcal{Z}^{(t)}, \mathcal{W}^*)}{\mathcal{L}(\boldsymbol{\Theta}^{(t-1)}, \mathcal{Z}^{(t)}, \mathcal{W}^{(t-1)})} \frac{q(\mathcal{W}^{(t-1)} | \mathcal{W}^*)}{q(\mathcal{W}^* | \mathcal{W}^{(t-1)})}.$$

At iteration $t - 1$, the SE Step can be run for an arbitrary large number of times to accelerate the exploration of the space of clustering configurations and so the convergence of the estimation algorithm to a stationary point. From our experience, we suggest to repeat the SE Step for at least 100 times per iteration.

- **M Step:** using the rows in $\mathcal{C}_k^{(t)}$ and the columns in $\mathcal{D}_r^{(t)}$, update the parameter estimates $\boldsymbol{\theta}_{kr}^{(t)}$ and $\boldsymbol{\phi}_r^{(t)}$. The derivative of the log-likelihood with respect to $(\boldsymbol{\theta}_{kr}, \boldsymbol{\phi}_r)$ does not lead to closed solutions for updating the model parameters, and for this reason a numerical optimizer must be applied. We exploit the L-BFGS-B algorithm

of Byrd *and others* (1995) implemented in the **stats** library of the **R** computing language, which allows constrained optimization; this aspect is particularly useful to estimate τ_{kr} under the identifiability constraint described in Section 3.1.

As pointed by Keribin *and others* (2015), the SE Step is not guaranteed to increase the classification log-likelihood at each iteration, but it generates an irreducible Markov chain with a unique stationary distribution which is expected to be concentrated around the ML parameter estimate. The estimation algorithm must be run for a large number of iterations. The final estimates of $(\hat{\Theta}, \hat{\mathcal{Z}}, \hat{\mathcal{W}})$ are the values obtained at the iteration from which (4) is maximum.

3.3 Model selection

SPARTACo can be run with different spatial covariance models $k(\cdot; \cdot)$ and with different combinations of K and R . We consider the problem of selecting the best model for the data, both in terms of the number of clusters and the spatial covariance function, using an information criterion. The most common criteria, the AIC and the BIC, cannot be derived under Model (1) because the likelihood of the data $p(\mathbf{X}; \Theta)$, marginalized with respect to the latent variables \mathcal{Z} and \mathcal{W} , is not available in closed form.

In this work, we propose to guide the model selection using the *integrated complete log-likelihood* (ICL, Biernacki *and others*, 2000). The ICL is a well-established criterion for selecting the number of clusters (Bouveyron *and others*, 2019) which has become popular in the co-clustering framework for selecting the size of LBM (Keribin *and others*, 2015; Bouveyron *and others*, 2017; Casa *and others*, 2021). Under Model (1) - (2), its expression is

$$\text{ICL} = \log \mathcal{L}(\hat{\Theta}, \hat{\mathcal{Z}}, \hat{\mathcal{W}}) - n \log K - p \log R - \frac{4KR + \dim(\phi)R}{2} \log np, \quad (5)$$

where $\dim(\phi)$ is the dimension of the of parameter vector ϕ_r , which does not depend on r . The derivation of (5) is described more in details in Section 1 of the Supplementary Material. Operatively, the best model from a list of candidates corresponds to the one with the largest value of (5).

In the presence of mixed effects, Delattre *and others* (2014) argue that the actual sample size is not trivial to define, and thus the classical information criteria need to be modified. In particular, they derive an alternative formulation of the BIC which includes a term that depends only from the parameters involved with the random effects. However, their model specification assumes that the marginal distribution of the data with the random parameters integrated out cannot be derived in closed form. Although the presence of the random variances $\sigma_{kr,i}^2$ makes SPARTACo a random effect model, the integration of $\sigma_{kr,i}^2$ from the density function of $\mathbf{x}_i^{kr} | \sigma_{kr,i}^2$ leads to the marginal density (3).

For this reason, we do not implement any modification based on the random effects into our information criterion (5).

4 Simulation studies

4.1 Simulation model

We study the performance of SPARTACo with five simulated spatial experiments that recreate some possible scenarios that can be found in real data. We generate the latent blocks using the matrix-variate Normal distribution (Gupta and Nagar, 2018) as follows: given the number of row and column clusters K^{true} and R^{true} (for convenience, we considered here $K^{\text{true}} = R^{\text{true}} = 3$ in every simulation experiment), the clustering labels $\mathcal{Z}^{\text{true}}$ and $\mathcal{W}^{\text{true}}$, and the clusters $\mathcal{C}_k^{\text{true}} = \{i = 1, \dots, n : \mathcal{Z}_i^{\text{true}} = k\}$ and $\mathcal{D}_r^{\text{true}} = \{j = 1, \dots, p : \mathcal{W}_j^{\text{true}} = r\}$, the (k, r) -th block is drawn from

$$\mathbf{X}^{kr} \sim \mathcal{MVN}(\mu_{kr}^{\text{true}} \mathbf{1}_{n_k \times p_r}, \Sigma_{kr}^{\text{true}}, \Delta_{kr}^{\text{true}}), \quad \Delta_{kr}^{\text{true}} = \tau_{kr}^{\text{true}} \mathcal{K}_r^{\text{true}}(\mathbf{S}^r; \boldsymbol{\phi}_r^{\text{true}}) + \xi_{kr}^{\text{true}} \mathbb{I}_{p_r}, \quad (6)$$

where $\mathcal{K}_r^{\text{true}}(\mathbf{S}^r; \boldsymbol{\phi}_r) = (k_r^{\text{true}}(\|\mathbf{s}_j^r - \mathbf{s}_{j'}^r\|; \boldsymbol{\phi}_r^{\text{true}}))_{1 \leq j, j' \leq p_r}$, and $k_r^{\text{true}}(\cdot; \boldsymbol{\phi}_r^{\text{true}})$ is an isotropic spatial covariance kernel parametrized by $\boldsymbol{\phi}_r^{\text{true}}$. Note that, differently from (2), the presence of the subscript r into the kernel matrix $\mathcal{K}_r^{\text{true}}$ denotes that the spatial covariance function can be different for any column cluster. In our simulations, we employed the *Exponential* kernel with scale θ_E for the columns in $\mathcal{D}_1^{\text{true}}$, the *Rational Quadratic* kernel with parameters (α_R, θ_R) for the columns in $\mathcal{D}_2^{\text{true}}$, and the *Gaussian* kernel (known also as *Squared Exponential*) with scale θ_G for the columns in $\mathcal{D}_3^{\text{true}}$. Their formulation is reported in Section 2 of the Supplementary Material and it is further discussed in Chapter 4 or Rasmussen and Williams (2006).

We took the sets of spatial coordinates $(\mathbf{S}_1, \dots, \mathbf{S}_{R^{\text{true}}})$ from the brain tissue sample of the subject with ID 151507 contained in the R package `spatialLIBD` and processed with Visium. As we briefly discussed in Section 1.1, the spots in these experiments have been manually annotated into layers. We extracted 200 spots from each of the three layers appearing in the top-right region of the image. The resulting map of 600 spots is shown in the left plot of Figure 3; the clustering labels $\mathcal{W}^{\text{true}}$ correspond to the labels assigned with the manual annotation. In addition, the right plot of Figure 3 shows the covariance functions used for the simulations. We set the covariance parameters $(\theta_E, \alpha_R, \theta_R, \theta_G)$ according to how much the clusters extend over the plane: the larger is the distance covered by a cluster, the sharper is the decay of the covariance function. Details are given in the caption of Figure 3.

Last, we set the values of the spatial signal-to-noise ratios $\tau_{kr}^{\text{true}} / \xi_{kr}^{\text{true}}$. The additional constraint $\tau_{kr}^{\text{true}} + \xi_{kr}^{\text{true}} = c_{kr}^{\text{true}}$ leads to a unique value of the parameters τ_{kr}^{true} and ξ_{kr}^{true} . Note that, due to the identifiability issue described in Section 3.1, which holds also for

the simulation model, the value assigned to c_{kr}^{true} is in practice irrelevant. For this reason, without loss of generality we assumed $c_{kr}^{\text{true}} = c^{\text{true}} = 10$, for any k and r .

In our simulations, we considered three cases: (i) no spatial effect, $\tau_{kr}^{\text{true}}/\xi_{kr}^{\text{true}} = 0$; (ii) the spatial effect is as much as the nugget effect, $\tau_{kr}^{\text{true}}/\xi_{kr}^{\text{true}} = 1$; and (iii) the spatial effect is considerably larger than the nugget effect, $\tau_{kr}^{\text{true}}/\xi_{kr}^{\text{true}} = 3$. Finally, we set $\mu_{kr}^{\text{true}} = 0$ to test if SPARTACo is able to recover the co-clusters using the covariance of the data without being driven by the effect of the mean.

4.2 Competing models and evaluation criteria

We fit SPARTACo on the simulated data using the exponential kernel, which has a lower decay than the more common Gaussian kernel considered by Svensson *and others* (2018) and Sun *and others* (2020). The estimation is carried running the algorithm described in Section 3.2 five times in parallel to avoid local maxima. The procedure is run for 5,000 iterations, and if the classification log-likelihood function is still growing, it is run until reaching 10,000 iterations. In addition to SPARTACo, we consider also the following co-clustering models:

- two independent k-means, applied separately to the rows and to the columns of the data matrix, using the R function `kmeans`;
- the biclustering algorithm BC, and its sparse version SPARSEBC with $\lambda = 1, 10, 20$, using the R package `sparseBC`;
- the matrix variate normal algorithm MVNB with the following setups: 1) $\lambda = 1$, $\rho_{\Sigma} = \rho_{\Delta} = 0.25$, 2) $\lambda = 10$, $\rho_{\Sigma} = \rho_{\Delta} = 2.5$ and 3) $\lambda = 20$, $\rho_{\Sigma} = \rho_{\Delta} = 5$. We had to implement a slight modification of the function `matrixBC` contained in the R package `sparseBC`, as its original form could not handle the computation of the logarithm of the determinant of some matrices.
- LBM, using the R package `blockcluster`;

Tan and Witten (2014) do not give any indication on how to select the penalization parameters ρ_{Σ} and ρ_{Δ} of MVNB. In their simulation experiments and real data applications, they simply set λ to be much larger than ρ_{Σ} and ρ_{Δ} . For this reason, in our simulations we fit MVNB with three setups, where the λ values are the same of SPARSEBC, and ρ_{Σ} and ρ_{Δ} are taken equal to a quarter of λ . The clustering accuracy is measured with the *clustering error rate* (CER, Chipman and Tibshirani, 2005; Witten and Tibshirani, 2009), an index that measures the disagreement between the clusters from the model and the true clustering labels: the closer is CER to 0, the larger is the agreement between the true and the estimated clusters. We measure the CER on both the rows and the columns.

In this section, we do not focus on the parameter estimates returned by SPARTACo, because the principal goal is evaluating the classification accuracy of the models. We leave the interpretation of the parameters to Section 5.

4.3 Simulation 1

We generated 9 blocks of size $n_k = 200 \times p_r = 200$, for every k and r . We assume that the variances and covariances of the genes do not change with respect to the spot clusters, thus $\Sigma_{kr}^{\text{true}} = \Sigma_k^{\text{true}}$ for all r . We draw Σ_k^{true} as follows:

$$\Sigma_1^{\text{true}} \sim \mathcal{W}(210, 0.03\mathbb{I}_{200}), \quad \Sigma_2^{\text{true}} \sim \mathcal{W}(230, 0.05\mathbb{I}_{200}), \quad \Sigma_3^{\text{true}} \sim \mathcal{W}(200, \Sigma_1^{\text{true}}/150), \quad (7)$$

where $\mathcal{W}(a, \mathbf{b})$ denotes a Wishart distribution with degrees of freedom a and scale matrix \mathbf{b} . Generating the covariance matrices from a Wishart distribution ensures that the draws are positive definite. The simulation setup in Formula (7) was selected after both numerical and graphical evaluations. More details on the motivations which led to this setup are given in Section 3 of the Supplementary Material.

We designed a spatial experiment in which three clusters of genes have a grade of spatial expression which change in three different areas of the tissue sample. The tessellation of the data matrix into blocks and the values of the spatial signal-to-noise ratios appear in Figure 4 (a). We simulated 10 replicates of this experiment and we fitted the co-clustering models listed in Section 4.2 using $K = R = 3$. The boxplots of the row and the column CER over the 10 replicates appear in the first line of Figure 5. SPARTACo outperforms the competing models and leads to no clustering errors. Good results on the rows are achieved also by the LBM, while on the columns the k-means type algorithms (K-MEANS, BC and SPARSEBC) and the MVNB with $\rho_{\Sigma} = \rho_{\Delta} = 5$ perform better than the other competitors.

This experiment has demonstrated that the presence of spatial covariance patterns, if not properly accounted for, heavily impacts on the performance of the standard co-clustering models. Since the MVNB is designed to flexibly estimate the covariance of the blocks, in theory it should be the best candidate for such complex experiments. However, results have shown that the smallest classification error is reached when the penalization parameters ρ_{Σ} and ρ_{Δ} are large, which results in diagonal estimated matrices $\hat{\Sigma}_k^{\text{MVNB}}$ and $\hat{\Delta}_r^{\text{MVNB}}$.

Furthermore, we tested the model selection criterion based on the ICL proposed in Section 3.3. Using the same 10 replicates of the experiment, we ran SPARTACo with K and R taking values in $\{2, 3, 4\}$. Supplementary Figure 3 shows that the proposed ICL always selects the correct model dimension, while the classification log-likelihood favors models with a larger number of co-clusters than the truth.

4.4 Simulation 2

The second simulation experiment differs from the first in the values of the spatial signal-to-noise ratios, which are now taken as in Figure 4 (b). For any r , the signal-to-noise ratios $\{\tau_{kr}^{\text{true}}/\xi_{kr}^{\text{true}}, k = 1, \dots, K\}$ have all the same value. As a consequence, $\Delta_{kr}^{\text{true}} = \Delta_r^{\text{true}}$ for any k . Under the current setup, the marginal distribution of a row $i \in \mathcal{C}_k^{\text{true}}$ given by the model generator of the data is

$$\mathbf{x}_{i\cdot}^k | \mathcal{Z}^{\text{true}}, \mathcal{W}^{\text{true}} \sim \mathcal{N}_p \left\{ \mathbf{0}, \Sigma_{ii}^{\text{true}} \text{diag}(\Delta_r^{\text{true}})_{r=1,2,3} \right\}, \quad (8)$$

where $\Sigma_{ii}^{\text{true}}$ is the variance parameter of the i -th row and does not depend on k , and $\text{diag}(\Delta_r^{\text{true}})_{r=1,2,3}$ is a block diagonal matrix formed by the matrices $\Delta_1^{\text{true}}, \dots, \Delta_3^{\text{true}}$. From Formula (8) it is clear that the marginal distribution of the rows does not carry any information about the row clusters. The only discriminating facet is the covariance between the rows: if $i, i' \in \mathcal{C}_k^{\text{true}}$, then $\text{Cov}(\mathbf{x}_{i\cdot}^k, \mathbf{x}_{i'\cdot}^k) = \Sigma_{k,ii'}^{\text{true}} \text{diag}(\Delta_r^{\text{true}})_{r=1,2,3}$, otherwise $\text{Cov}(\mathbf{x}_{i\cdot}^k, \mathbf{x}_{i'\cdot}^k) = \mathbf{0}$.

We ran the co-clustering models using $K = R = 3$ on 10 replicates on the proposed experiment; the results are displayed in the second line of Figure 5. Our model outperforms the competitors: on the rows, the median CER from SPARTACo is 0.2, while on the columns it returns a perfect classification on all replicates. Both Simulations 1 and 2 have shown that SPARTACo works properly even if the spatial covariance function employed by the fitted model in Formula 2 does not match the covariance functions of the data generating process. In particular, Experiment 2 has highlighted this remarkable result because the only cluster of columns for which the spatial covariance function is correctly specified is $r = 1$, which however is devoid of any spatial effect, as $\tau_{k1}^{\text{true}} = 0$ for any k .

The best competitor on the rows is the LBM, with a median CER of 0.42. On the columns, the best results are from the k-means type models, or alternatively from the MVNB with $\lambda = 20$ and $\rho_{\Sigma} = \rho_{\Delta} = 5$. This experiment hence confirms what we have already observed in Simulation 1, namely that, in the presence of spatial covariance patterns in the data, the model of Tan and Witten (2014) tends to fail in recovering the correlation structure, at least in our simulation setup. This is demonstrated by the diagonal estimated covariance matrices $\{\hat{\Sigma}_k^{\text{MVNB}}, k = 1, 2, 3\}$ and $\{\hat{\Delta}_r^{\text{MVNB}}, r = 1, 2, 3\}$.

4.5 Simulation 3

The third simulation experiment assumes that the spatial signal-to-noise ratio $\tau_{kr}^{\text{true}}/\xi_{kr}^{\text{true}}$ is constant across the blocks within the same row cluster k ; as a consequence, $\tau_{kr} = \tau_k$ for any r . This case is illustrated in Figure 4 (c). Notice for example that the rows in $\mathcal{C}_1^{\text{true}}$ are not spatially expressed in any of the three column clusters.

Under the current simulation setup, the marginal distribution of the column $j \in \mathcal{D}_r^{\text{true}}$

given by the generative model is

$$\mathbf{x}_{\cdot j}^r | \mathcal{Z}^{\text{true}}, \mathcal{W}^{\text{true}} \sim \mathcal{N}_n \left\{ \mathbf{0}, c^{\text{true}} \text{diag}(\Sigma_k^{\text{true}})_{k=1,2,3} \right\},$$

and so the marginal distribution of j is not informative on the column clusters. The only discriminating facet is the covariance across the columns: if $j, j' \in \mathcal{D}_r^{\text{true}}$, then $\text{Cov}(\mathbf{x}_{\cdot j}^r, \mathbf{x}_{\cdot j'}^r) = \text{diag}\{\tau_k^{\text{true}} k_r^{\text{true}} (||\mathbf{s}_j^r - \mathbf{s}_{j'}^r||; \phi_r^{\text{true}}) \Sigma_k^{\text{true}}\}_{k=1,2,3}$; if instead $j \in \mathcal{D}_r^{\text{true}}$ and $j' \in \mathcal{D}_{r'}^{\text{true}}$, then $\text{Cov}(\mathbf{x}_{\cdot j}^r, \mathbf{x}_{\cdot j'}^r) = \mathbf{0}$.

We ran the co-clustering models on 10 replicates of the experiment using $K = R = 3$; the results appear in the third line of Figure 5. On the rows, SPARTACo outperforms the competitor models returning a CER of zero for all replicates. On the columns, its clustering accuracy is highly variable: the median CER is 0.21, the third and the first quartiles are 0.08 and 0.25, and extremes are 0 and 0.36. The competitor models, and in particular the k-means type models, are substantially less variable than SPARTACo. Their median column CER is 0.13. However, none of them ever returns a perfect classification.

Even if SPARTACo has returned unstable results on the columns, the advantages brought by our model against the competitors are many, and are particularly visible from the results on the rows. The column clustering changes considerably across the replicates because, in the current setup, our estimation algorithm is more sensible to the starting points. From our experience, if independent runs of the estimation algorithm reach distant stationary points, both the number of starting points and the number of iterations of the SE Step should be increased to favor a faster exploration of the space of the configurations.

4.6 Simulation 4

Up to now, we built the simulation experiments under the framework in which SPARTACo is designed to work properly, that is the case where the genes/spots in a cluster are correlated only with the other genes/spots of the same cluster. In this section, we violate this assumption and we design a spatial experiment where both the genes and the spots are correlated also with genes and spots from other clusters. This experiment aims to study the effects of an additional dependency structure across the data that is not accounted by the fitted model.

Let \mathbf{X}_s be a 600×600 spatial experiment made of 9 equally sized blocks, generated as in Simulation 1, and $\mathbf{X}_b \sim \mathcal{MVN}(\mathbf{0}, \Sigma_b, \Delta_b)$. Both Σ_b and Δ_b are squared matrices of size 600: the first is drawn from $\Sigma_b \sim \mathcal{W}(600, 0.015\mathbb{I}_{600})$, the second is $\Delta_b = \tau_b \mathcal{K}^b(\mathbf{S}; \sigma_b)$, where $\mathcal{K}^b(\mathbf{S}; \sigma_b) = (k^b(||\mathbf{s}_j - \mathbf{s}_{j'}||; \sigma_b))_{1 \leq j, j' \leq 600}$ and $k^b(\cdot; \sigma_b)$ is a Gaussian kernel with scale σ_b . We set $\tau_b = c^{\text{true}}/2$ and $\sigma_b = 50$. The final simulation experiment is made as follows: $\mathbf{X} = \lambda_s \mathbf{X}_s + \lambda_b \mathbf{X}_b$, where $\lambda_s, \lambda_b \geq 0$. We generated 10 replicates of the current experiment, each time drawing first the matrices \mathbf{X}_s and \mathbf{X}_b , and then combining them to form \mathbf{X} . Supplementary Figure 4 shows a single realization of \mathbf{X}_s , \mathbf{X}_b and \mathbf{X} using

$\lambda_s = \lambda_b = \sqrt{0.5}$. This value satisfies the constraint $\lambda_s^2 + \lambda_b^2 = 1$ that we imposed to keep the variance of the current experiment comparable with the previous experiments proposed in this work.

We ran the co-clustering models using $K = R = 3$; results appear in the last row of Figure 5. Despite the additional correlation structure in the data brought by the nuisance signal \mathbf{X}_b , SPARTACo outperforms its competitors on both the row and the column clustering. In the right plot, the CER boxplots are more variable than in the left plot, therefore, the nuisance component has affected more the column than the row clustering of the employed models. Among the competitors, K-MEANS and MVNB with $\lambda = 10$ and $\rho_{\Sigma} = \rho_{\Delta} = 2.5$ are the least affected by the nuisance: the former because it performs the clustering on the two dimension of the data matrix separately, the latter because it regulates the estimate of the row and column covariances with a moderate shrinkage factor.

4.7 Simulation 5

In the last experiment, we violate the assumption that the latent block structure corresponds to a segmentation of the data matrix into K row clusters and R column clusters. For instance, we generate a spatial experiment creating first the R column clusters, and then generating the K row clusters independently for each column cluster. From a biological perspective, this setup simulates the case where the expression of some genes is comparable only in some specific areas of the tissue sample.

Let $\mathcal{C}_{kr}^{\text{true}}$ and $\mathcal{D}_r^{\text{true}}$ be the actual row and column clusters, with $k = 1, \dots, K$ and $r = 1, \dots, R$, where $\mathcal{C}_{kr}^{\text{true}} = \{i = 1, \dots, n : \mathcal{Z}_{ir}^{\text{true}} = k\}$ is the k -th row cluster within the r -th column cluster, and $|\mathcal{C}_{kr}^{\text{true}}| = n_{kr}$. Under the current setup, we drew $\mathbf{X}^{kr} \sim \mathcal{MVN}(\mathbf{0}, \Sigma_{kr}^{\text{true}}, \Delta_{kr}^{\text{true}})$. Notice that, differently from Section 4.3, the covariance matrices of the rows $\Sigma_{kr}^{\text{true}}$ change with respect to r because the number of observations in the cluster is n_{kr} (and no longer n_k). The tessellation of the data matrix into blocks is shown in Figure 4 (d). The size of the clusters is $n_{kr} = 200$ for $k = 1, 2, 3$ and $r = 1, 2$, while $n_{13} = 100$, $n_{23} = 200$ and $n_{33} = 300$. The covariance matrices of the rows are drawn as follows:

$$\Sigma_{1r}^{\text{true}} \sim \mathcal{W}(n_{1r} + 10, 0.03\mathbb{I}_{n_{1r}}), \quad \Sigma_{2r}^{\text{true}} \sim \mathcal{W}(n_{2r} + 30, 0.05\mathbb{I}_{n_{2r}}), \quad \Sigma_{3r}^{\text{true}} \sim \mathcal{W}(n_{3r}, \Sigma_{3r}^*/150),$$

where $\Sigma_{3r}^* \sim \mathcal{W}(n_{3r} + 10, 0.03\mathbb{I}_{n_{3r}})$. Notice that this setting is nothing but a generalization of what appears in Formula (7). Finally, the employed spatial signal-to-noise ratio values $\{\tau_{kr}/\xi_{kr}\}$ are shown in Figure 4 (e).

To facilitate the model evaluation and the interpretation of the results, we assign to every row i an alternative clustering label $\mathcal{Z}_i^{\text{true}}$ such that $\mathcal{Z}_i^{\text{true}} = \mathcal{Z}_{i'}^{\text{true}}$ if $i, i' \in (\mathcal{C}_{k_11}^{\text{true}} \cap \mathcal{C}_{k_22}^{\text{true}} \cap \mathcal{C}_{k_33}^{\text{true}})$, for some $k_1, k_2, k_3 \in \{1, 2, 3\}$. In words, this means that the new

clusters are formed by the rows that belong to the same cluster in all of the three column clusters. The new row clustering labels appear on the right side of Figure 4 (d). In our experiment, every $\mathcal{Z}_i^{*\text{true}} \in \{1, \dots, 6\}$, and $\mathcal{C}_b^{*\text{true}} = \{i = 1, \dots, n : \mathcal{Z}_i^{*\text{true}} = b\}$ is the b -th alternative cluster with size $|\mathcal{C}_b^{*\text{true}}| = 100$, for $b = 1, \dots, 6$.

To reduce the computational cost spent on the simulation, we generated a single replicate of the experiment, and we fitted SPARTACo using $K = 3, \dots, 10$, while the number of column clusters is kept equal to its real value, $R = 3$. Supplementary Figure 5 shows that the ICL criterion selects $K = 7$ as the optimal model dimension; using the log-likelihood, we would have wrongly picked $K = 10$, confirming the importance of using a suitable information criterion. The selected model returns a row CER of 0.015 and a column CER of 0. In details, the model correctly recovers the clusters $\mathcal{C}_2^{*\text{true}}, \dots, \mathcal{C}_5^{*\text{true}}$ and almost the entire $\mathcal{C}_6^{*\text{true}}$, except for one observation that is assigned to $\mathcal{C}_5^{*\text{true}}$. Lastly, $\mathcal{C}_1^{*\text{true}}$ is split into two groups of almost equal size.

We finally run the competing models using $K = 7$ and $R = 3$. The second best result is reached by the LBM, which returned a poor clustering of the columns (CER = 0.182) and a good clustering of the columns (CER = 0)

5 Application

In this section, we analyze the human dorsolateral pre-frontal cortex sample from the subject 151673 studied by Maynard *and others* (2021) that we briefly described in Section 1.1 and shown in Figure 1. The dataset has 33,538 genes measured over 3,639 spots. Similarly to 10X-scRNA-seq protocols, 10X-Visium yields *unique molecular identifier* (UMI) counts as gene expression values. The region on the bottom-left corner of the tissue is an area of large gene expression activity, with an average of 3,733 UMI counts per spot, measured over 1,585 spots (Figure 6 (a)). For this and computational reasons, we restricted our attention to this part of the image.

As a first step, we sought to exclude uninformative genes and reduce the analysis to a lower dimensional problem. We applied the gene selection procedure for UMI count data proposed by Townes *and others* (2019), i.e., we fit a multinomial model on every vector of gene expression and compute the deviance. Based on the criterion that large deviance values are associated to informative genes, we kept the first 1,000 genes and discarded the remaining ones. Supplementary Figure 6 shows that the deviance, which is very high for the top genes, reaches a plateau after 200 genes. To normalize the data, we computed, for each selected gene, the Pearson residuals based on the binomial approximation of the multinomial distribution as done in Townes *and others* (2019). The result of this procedure is the expression matrix \mathbf{X} whose entries are $x_{ij} \in \mathbb{R}$ and whose row vectors \mathbf{x}_i yield approximately symmetric histograms.

We fitted SPARTACo with all the configurations in $\{(K, R) : K = 1, 2, 3, R =$

$4, \dots, 8\}$. The range of K values was chosen to investigate the absence of gene clusters ($K = 1$) against the presence of two or three groups. However, when estimating our model with $K = 3$, we obtained only two non-empty clusters for all $R > 4$ configurations. This indicates that our model finds evidence of only two groups of genes in these data. The range of column cluster values reflects the results of Maynard *and others* (2021), who found three major layers in this area and two small layers in the top-left. Even though we do not expect that the clustering of SPARTACo perfectly matches the cortical layers, we believe that their number is indicative of the biological diversity of this specific area.

The ICL criterion selects $K = 2$ and $R = 8$. We did not explore values of R greater than 8 as this would result in too many small clusters, reducing the biological interpretation. Figure 6 (b) displays the 1,585 spots colored according to the estimated clusters, which follow a morphology similar to the cortical layers. Clusters \mathcal{D}_1 , \mathcal{D}_2 and \mathcal{D}_4 are all within the White Matter, while \mathcal{D}_8 is placed at the border between the White Matter and Layer 6. The remaining clusters cover the rest of the surface, occupied almost entirely by Layers 5 and 6. Panels (c) and (d) in Figure 6 display the estimated block structure of the matrix experiment and the estimated means $\hat{\mu}_{kr}$ (Panel (c)) and spatial signal-to-noise ratios $\hat{\tau}_{kr}/\hat{\xi}_{kr}$ (panel d). As for the row clustering, many of the genes in Cluster \mathcal{C}_2 ($n_2 = 234$) were ranked within the top 200 most informative genes by the deviance procedure of Townes *and others* (2019). In \mathcal{C}_2 , both the estimated means and spatial signal-to-noise ratios vary substantially across the 8 spot clusters. In particular, there is evidence of large spatial expression in \mathcal{D}_2 ($\hat{\tau}_{22}/\hat{\xi}_{22} = 1.12$) and moderate spatial expression in $\mathcal{D}_4, \dots, \mathcal{D}_7$ ($\hat{\tau}_{2r}/\hat{\xi}_{2r} \in [0.45, 0.73]$, for $r = 4, \dots, 7$), while it is small in the remaining areas. Thus, the coordinated spatial activity emerges both within the White Matter and in the cortical area, but not in the border spots. On the contrary, the genes in \mathcal{C}_1 ($n_1 = 766$) show a small spatial variation in every spot cluster, as $\hat{\tau}_{2r}/\hat{\xi}_{2r} \leq 0.22$ for all r , suggesting a constant expression of these genes throughout the tissue. In fact, \mathcal{C}_1 is enriched for housekeeping genes with respect to \mathcal{C}_2 (chi-square test, $p = 3.2 \times 10^{-6}$). Housekeeping genes are maintainers of the cellular functions and their activity is not restricted to a specific cell type (Eisenberg and Levanon, 2003). It is therefore expected that these genes show a small spatial variation across the tissue.

The co-clustering results discussed above allow us to answer the first two research questions listed in Section 1.1 that motivated our work. We now turn our attention to the third research question, namely the identification of genes that exhibit high specific variation. To do so, for every block (k, r) , we investigate the conditional random variables $\sigma_{kr,i}^2 | \mathbf{X}, \hat{\mathbf{Z}}, \hat{\mathbf{W}}$ to determine which genes are most highly variable in each block. We display their density in Supplementary Figures 7 and 8, highlighting in red the five genes with the largest $\mathbb{E}(\sigma_{kr,i}^2 | \text{data})$, for every k and r . We expect that genes with a large gene-specific variance in some areas are likely to be informative of the biological mechanisms occurring there.

Here, we only discuss genes in \mathcal{C}_2 , as these are the ones that exhibit the largest spatial expression. These genes show a cluster-specific pattern of expression, with different genes showing high variability in different spot clusters (Supplementary Figure 8). For instance, among the highly variable genes in \mathcal{D}_2 and \mathcal{D}_4 there are *MBP* and *PLP1*, which are responsible, respectively, for the production and the maintenance of myelin, the covering sheath of the nerve fibers in the White Matter. Conversely, among the highly variable genes in \mathcal{D}_7 , we notice *CCK* and *PCP4*: these are markers of distinct subtypes of excitatory neurons present in Layers 5-6 (Hodge *and others*, 2019).

Taken together, these results convincingly show that our model is able to partition the tissue in coherent clusters, which exhibit cluster-specific gene expression, both spatially coordinated and otherwise.

6 Discussion

The growing demand of appropriate statistical methods to analyze spatial transcriptomic experiments has driven us to introduce SPARTACo, a model-based co-clustering tool which groups genes with a similar profile of spatial expression in specific areas of a tissue. SPARTACo brings the concepts of spatial modelling into the co-clustering framework, and thus it can be applied to any dataset with entries in the real domain and whose row or column vectors are multivariate observations recorded at some fixed sites in space. The inference is carried out via maximization of the classification log-likelihood function. To do so, we put together two variants of the EM algorithm, the classification EM and the stochastic EM, forming what we called the classification-stochastic EM. We completed our proposal deriving the formulation of the ICL for our model to drive the model selection.

A series of simulation studies have highlighted that, in the presence of spatial covariance patterns, the major co-clustering models become inadequate to recover the hidden block structure of the data. On the contrary, SPARTACo have shown remarkable results in each simulation, managing to distinguish different spatial expression profiles in different areas of the image. It further revealed to be robust to the presence of a nuisance component into the data. Lastly, we demonstrated how our proposal is capable of answering specific biological research questions using a human brain tissue sample processed with the Visium protocol. Our model has identified two clusters of genes with different spatial expression profiles in eight different areas of the tissue. A subsequent downstream analysis has allowed us to determine the highly variable genes in each of the eight pinpointed areas.

Although this article has introduced a complete solution to answer some relevant questions in the analysis of spatial transcriptomics, we believe that there is space for further extensions. First, instead of relying on pre-processing techniques (Townes *and others*, 2019), SPARTACo could be extended to directly model UMI counts, similarly to

how SPARK (Sun *and others*, 2020) has extended SpatialDE (Svensson *and others*, 2018). Second, to overcome the limitations of the stochastic EM which appeared in Section 4.5, we could explore the *simulated annealing* algorithm (Van Laarhoven and Aarts, 1987), to reduce the chances of converging to local maxima.

7 Software

Software in the form of an R package that implements SPARTACo, together with the functions to simulate the data as in Section 4, is available online at <https://github.com/drighelli/spartaco>. The functions for selecting the informative genes and transforming the data using the procedure of Townes *and others* (2019) are implemented in the R package **scry**.

Acknowledgments

The authors are thankful to Giovanna Menardi and Alessandro Casa for the precious discussions on co-clustering and to Levi Waldron and Vince Carey for help with the framing of the biological questions. We finally thank Dario Righelli for his help with the software implementation. This work was supported in part by CZF2019-002443 (DR) from the Chan Zuckerberg Initiative DAF, an advised fund of Silicon Valley Community Foundation. The authors are supported by the National Cancer Institute of the National Institutes of Health (U24CA180996).

Conflict of Interest: None declared.

References

ALLEN, GENEVERA I. AND TIBSHIRANI, ROBERT. (2010). Transposable regularized covariance models with an application to missing data imputation. *The Annals of Applied Statistics* **4**(2), 764 – 790.

ANDERLUCCI, LAURA AND VIROLI, CINZIA. (2015). Covariance pattern mixture models for the analysis of multivariate heterogeneous longitudinal data. *The Annals of Applied Statistics* **9**(2), 777–800.

BENJAMINI, YOAV AND HOCHBERG, YOSEF. (1995). Controlling the false discovery rate: A practical and powerful approach to multiple testing. *Journal of the Royal Statistical Society: Series B (Methodological)* **57**(1), 289–300.

BIERNACKI, CHRISTOPHE, CELEUX, GILLES AND GOVAERT, GÉRARD. (2000). Assessing a mixture model for clustering with the integrated completed likelihood. *IEEE transactions on pattern analysis and machine intelligence* **22**(7), 719–725.

BOUVEYRON, CHARLES, BOZZI, LAURENT, JACQUES, JULIEN AND JOLLOIS, FRANÇOIS-XAVIER. (2017, December). The Functional Latent Block Model for the Co-Clustering of Electricity Consumption Curves. *Journal of the Royal Statistical Society: Series C (Applied Statistics)*.

BOUVEYRON, CHARLES, CELEUX, GILLES, MURPHY, T. BRENDAN AND RAFTERY, ADRIAN E. (2019). *Model-based clustering and classification for data science*, Cambridge Series in Statistical and Probabilistic Mathematics. Cambridge University Press, Cambridge. With applications in R.

BYRD, RICHARD H., LU, PEIHUANG, NOCEDAL, JORGE AND ZHU, CI YOU. (1995). A limited memory algorithm for bound constrained optimization. *SIAM Journal on Scientific Computing* **16**(5), 1190–1208.

CAPONERA, ALESSIA, DENTI, FRANCESCO, RIGON, TOMMASO, SOTTOSANTI, ANDREA AND GELFAND, ALAN. (2017). Hierarchical spatio-temporal modeling of resting state fmri data. In: *START UP RESEARCH*. Springer. pp. 111–130.

CASA, ALESSANDRO, BOUVEYRON, CHARLES, EROSHEVA, ELENA AND MENARDI, GIOVANNA. (2021). Co-clustering of time-dependent data via shape invariant model. *arXiv preprint arXiv:2104.03083*.

CELEUX, GILLES AND GOVAERT, GÉRARD. (1992). A classification em algorithm for clustering and two stochastic versions. *Computational statistics & Data analysis* **14**(3), 315–332.

CHEN, KOK HAO, BOETTIGER, ALISTAIR N., MOFFITT, JEFFREY R., WANG, SIYUAN AND ZHUANG, XIAOWEI. (2015). Spatially resolved, highly multiplexed rna profiling in single cells. *Science* **348**(6233), aaa6090.

CHIPMAN, HUGH AND TIBSHIRANI, ROBERT. (2005, 11). Hybrid hierarchical clustering with applications to microarray data. *Biostatistics* **7**(2), 286–301.

CRESSIE, NOEL. (2015). *Statistics for spatial data*. John Wiley & Sons.

DE LA CRUZ-MESÍA, ROLANDO AND MARSHALL, GUILLERMO. (2006, May). Non-linear random effects models with continuous time autoregressive errors: a bayesian approach. *Statistics in medicine* **25**(9), 1471–1484.

DELATTRE, MAUD, LAVIELLE, MARC, POURSAT, MARIE-ANNE *and others*. (2014). A note on bic in mixed-effects models. *Electronic journal of statistics* **8**(1), 456–475.

DRIES, RUBEN, ZHU, QIAN, DONG, RUI, ENG, CHEE-HUAT LINUS, LI, HUIPENG, LIU, KAN, FU, YUNTIAN, ZHAO, TIANXIAO, SARKAR, ARPAN, BAO, FENG *and others*. (2021). Giotto: a toolbox for integrative analysis and visualization of spatial expression data. *Genome biology* **22**(1), 1–31.

EDSGÄRD, DANIEL, JOHNSSON, PER AND SANDBERG, RICKARD. (2018). Identification of spatial expression trends in single-cell gene expression data. *Nature methods* **15**(5), 339–342.

EFRON, BRADLEY. (2009). Are a set of microarrays independent of each other? *The Annals of Applied Statistics* **3**(3), 922–942.

EISENBERG, ELI AND LEVANON, EREZ Y. (2003). Human housekeeping genes are compact. *TRENDS in Genetics* **19**(7), 362–365.

GAETAN, CARLO AND GUYON, XAVIER. (2010). *Spatial statistics and modeling*, Volume 90. Springer.

GOVAERT, GÉRARD AND NADIF, MOHAMED. (2008). Block clustering with Bernoulli mixture models: comparison of different approaches. *Computational Statistics & Data Analysis* **52**(6), 3233–3245.

GOVAERT, GÉRARD AND NADIF, MOHAMED. (2010). Latent block model for contingency table. *Communications in Statistics. Theory and Methods* **39**(3), 416–425.

GOVAERT, GÉRARD AND NADIF, MOHAMED. (2013). *Co-clustering: models, algorithms and applications*. John Wiley & Sons.

GUPTA, ARJUN K AND NAGAR, DAYA K. (2018). *Matrix variate distributions*, Volume 104. CRC Press.

HODGE, REBECCA D, BAKKEN, TRYGVE E, MILLER, JEREMY A, SMITH, KIMBERLY A, BARKAN, ELIZA R, GRAYBUCK, LUCAS T, CLOSE, JENNIE L, LONG, BRIAN, JOHANSEN, NELSON, PENN, OSNAT *and others*. (2019). Conserved cell types with divergent features in human versus mouse cortex. *Nature* **573**(7772), 61–68.

HU, KENNETH H., EICHORST, JOHN P., MCGINNIS, CHRIS S., PATTERSON, DAVID M., CHOW, ERIC D., KERSTEN, KELLY *and others*. (2020). Zipseq: barcoding for real-time mapping of single cell transcriptomes. *Nature methods* **17**(8), 833–843.

KERIBIN, CHRISTINE, BRAULT, VINCENT, CELEUX, GILLES AND GOVAERT, GÉRARD. (2015). Estimation and selection for the latent block model on categorical data. *Statistics and Computing* **25**(6), 1201–1216.

LUBECK, ERIC, COSKUN, AHMET F, ZHIYENTAYEV, TIMUR, AHMAD, MUBHIJ AND CAI, LONG. (2014). Single-cell in situ rna profiling by sequential hybridization. *Nature methods* **11**(4), 360–361.

MAYNARD, KRISTEN R., COLLADO-TORRES, LEONARDO, WEBER, LUKAS M., UYTINGCO, CEDRIC, BARRY, BRIANNA K., WILLIAMS, STEPHEN R. and others. (2021). Transcriptome-scale spatial gene expression in the human dorsolateral prefrontal cortex. *Nature Neuroscience*.

MORAN, GEMMA E., ROČKOVÁ, VERONIKA AND GEORGE, EDWARD I. (2021). Spike-and-slab Lasso biclustering. *The Annals of Applied Statistics* **15**(1), 148 – 173.

MURUA, ALEJANDRO AND QUINTANA, FERNANDO ANDRÉS. (2021). Biclustering via Semiparametric Bayesian Inference. *Bayesian Analysis*, 1 – 27.

NOBILE, AGOSTINO AND FEARNSIDE, ALASTAIR T. (2007). Bayesian finite mixtures with an unknown number of components: The allocation sampler. *Statistics and Computing* **17**(2), 147–162.

PARDO, BRENDA, SPANGLER, ABBY, WEBER, LUKAS M., HICKS, STEPHANIE C., JAFFE, ANDREW E., MARTINOWICH, KERI and others. (2021). spatialLIBD: an R/Bioconductor package to visualize spatially-resolved transcriptomics data. *bioRxiv*.

RAO, NIKHIL, CLARK, SHEILA AND HABERN, OLIVIA. (2020). Bridging genomics and tissue pathology. *Genetic Engineering & Biotechnology News* **40**(2), 50–51.

RASMUSSEN, CARL EDWARD AND WILLIAMS, CHRISTOPHER K. I. (2006). *Gaussian Processes for Machine Learning*. The MIT Press.

RIGHELLI, DARIO, WEBER, LUKAS M., CROWELL, HELENA L., PARDO, BRENDA, COLLADO-TORRES, LEONARDO, GHAZANFAR, SHILA and others. (2021). SpatialExperiment: infrastructure for spatially resolved transcriptomics data in R using bioconductor. *bioRxiv*.

RODRIGUES, SAMUEL G., STICKELS, ROBERT R., GOEVA, ALEKSANDRINA, MARTIN, CARLY A., MURRAY, EVAN, VANDERBURG, CHARLES R. and others. (2019). Slide-seq: A scalable technology for measuring genome-wide expression at high spatial resolution. *Science* **363**(6434), 1463–1467.

SMYTH, GORDON K. (2004). Linear models and empirical bayes methods for assessing differential expression in microarray experiments. *Statistical applications in genetics and molecular biology* **3**(1).

SUN, SHIQUAN, ZHU, JIAQIANG AND ZHOU, XIANG. (2020). Statistical analysis of spatial expression patterns for spatially resolved transcriptomic studies. *Nature methods* **17**(2), 193–200.

SVENSSON, VALENTINE, TEICHMANN, SARAH A. AND STEGLE, OLIVER. (2018). Spatialde: identification of spatially variable genes. *Nature methods* **15**(5), 343–346.

TAN, KEAN MING AND WITTEN, DANIELA M. (2014). Sparse biclustering of transposable data. *Journal of Computational and Graphical Statistics* **23**(4), 985–1008.

TIBSHIRANI, ROBERT. (1996). Regression shrinkage and selection via the lasso. *Journal of the Royal Statistical Society: Series B (Methodological)* **58**(1), 267–288.

TOWNES, F WILLIAM, HICKS, STEPHANIE C, ARYEE, MARTIN J AND IRIZARRY, RAFAEL A. (2019). Feature selection and dimension reduction for single-cell rna-seq based on a multinomial model. *Genome biology* **20**(1), 1–16.

VAN LAARHOVEN, PETER JM AND AARTS, EMILE HL. (1987). Simulated annealing. In: *Simulated annealing: Theory and applications*. Springer, pp. 7–15.

WITTEN, DANIELA M. AND TIBSHIRANI, ROBERT. (2009). Covariance-regularized regression and classification for high dimensional problems. *Journal of the Royal Statistical Society: Series B (Methodological)* **71**(3), 615–636.

WYSE, JASON AND FRIEL, NIAL. (2012). Block clustering with collapsed latent block models. *Statistics and Computing* **22**(2), 415–428.

ZHAO, EDWARD, STONE, MATTHEW R., REN, XING, GUENTHOER, JAMIE, SMYTHE, KIMBERLY S, PULLIAM, THOMAS and others. (2021). Spatial transcriptomics at sub-spot resolution with bayesspace. *Nature Biotechnology*, 1–10.

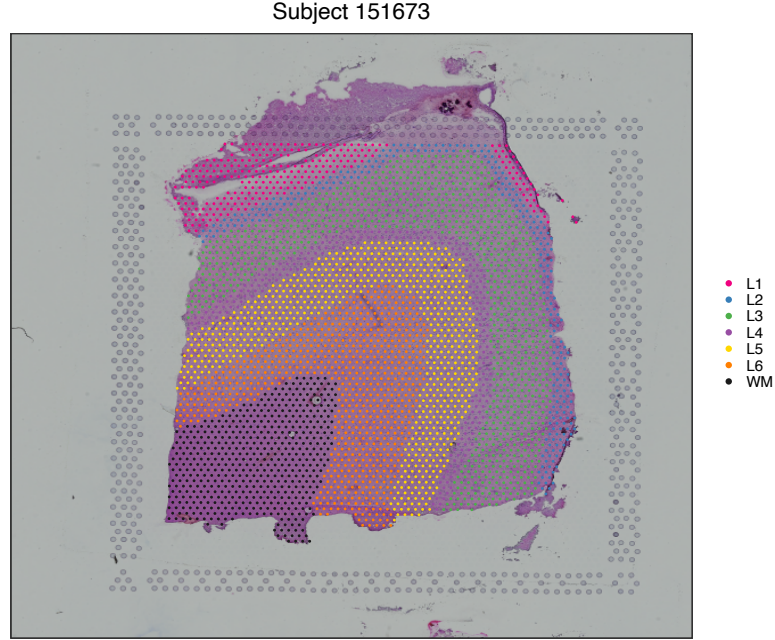


Figure 1: Tissue sample of LIBD human dorsolateral pre-frontal cortex (DLPFC) processed with Visium platform and stored in the R package `spatialLIBD`. The dots represent the spots over the chip surface. Different colors denote a manual annotation of the areas performed by Maynard *and others* (2021): they recognize 6 Layers (L1-L6) plus a White Matter (WM) stratum.

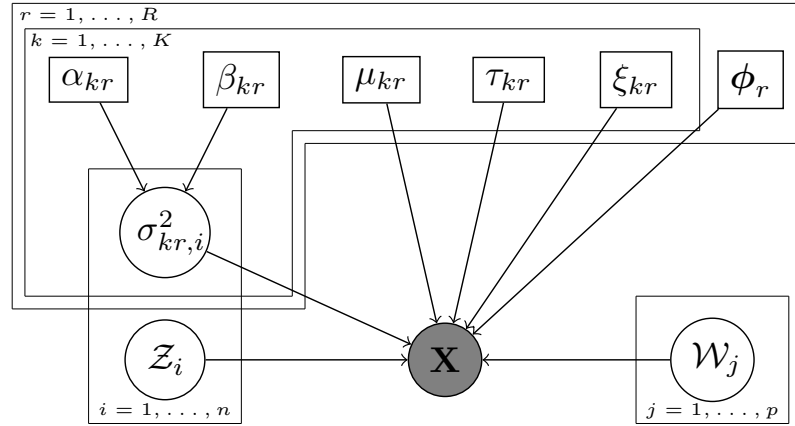


Figure 2: DAG of the co-clustering model. Grey circle denotes the data, white circles are the latent random variables, and white rectangles are the model parameters.

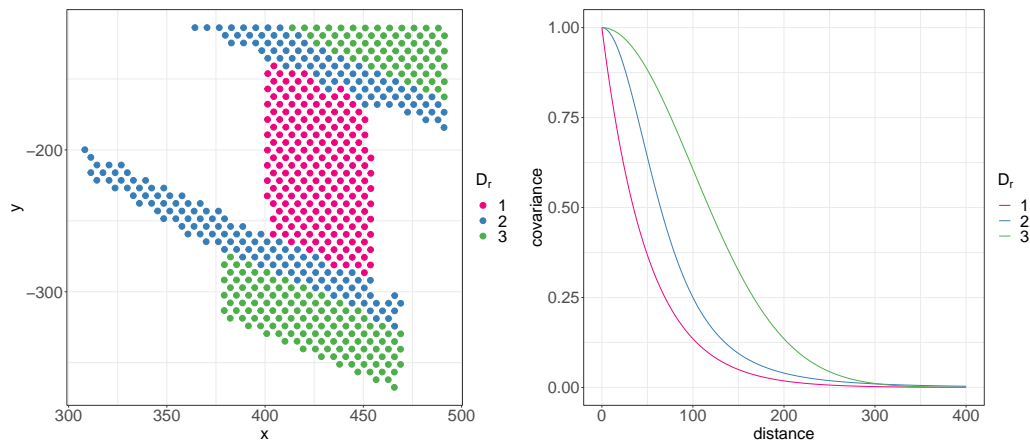


Figure 3: Left: map of the spots used to generate the simulation experiments, extracted from the subject 151507 contained in the R package `spatialLIBD`. The clusters are of equal size, $p_r = p_2 = p_3 = 200$. Right: comparison of the covariance functions used in the three clusters of spots. When $r = 1$, the covariance is Exponential with scale $\theta_E = 50$, when $r = 2$, it is rational quadratic with $\theta_R = 50$ and $\alpha_R = 2$, and when $r = 3$, it is Gaussian with scale $\theta_G = 100$.

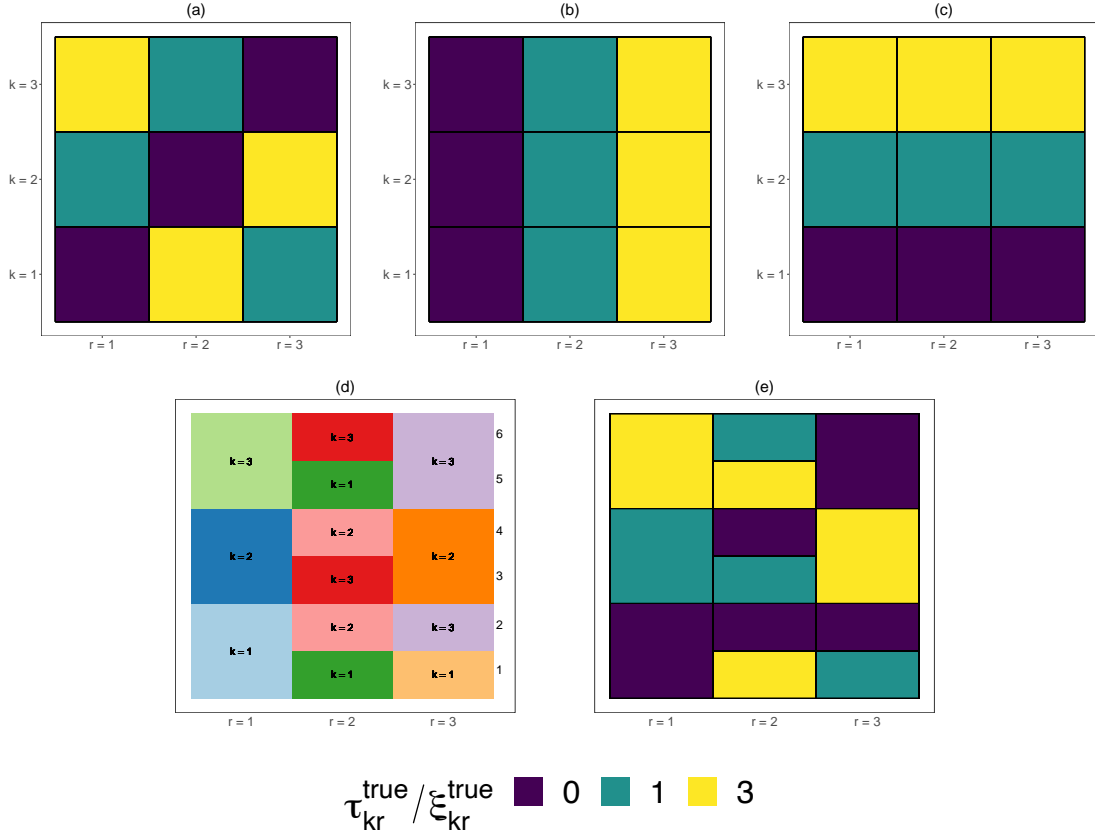


Figure 4: Representation of the latent block structures used to generate the simulation experiments. All the blocks in Panels (a)-(c) have the same size and are colored according to the value of the spatial signal-to-noise ratio $\tau_{kr}^{\text{true}} / \xi_{kr}^{\text{true}}$. The setup in Panel (a) is used for Simulations 1 and 4, Panel (b) is used for Simulation 2, Panel (c) for Simulation 3 and Panel (d) for Simulation 5. Panel (d) gives the hidden block structure of Simulation 5. Within the columns 1 and 2, the row clusters have the same size (200), while in the third column it is $n_{13} = 100$, $n_{23} = 200$ and $n_{33} = 300$. The numbers from 1 to 6 on the right denote the alternative clusters $\mathcal{C}_1^{\text{true}}, \dots, \mathcal{C}_6^{\text{true}}$.

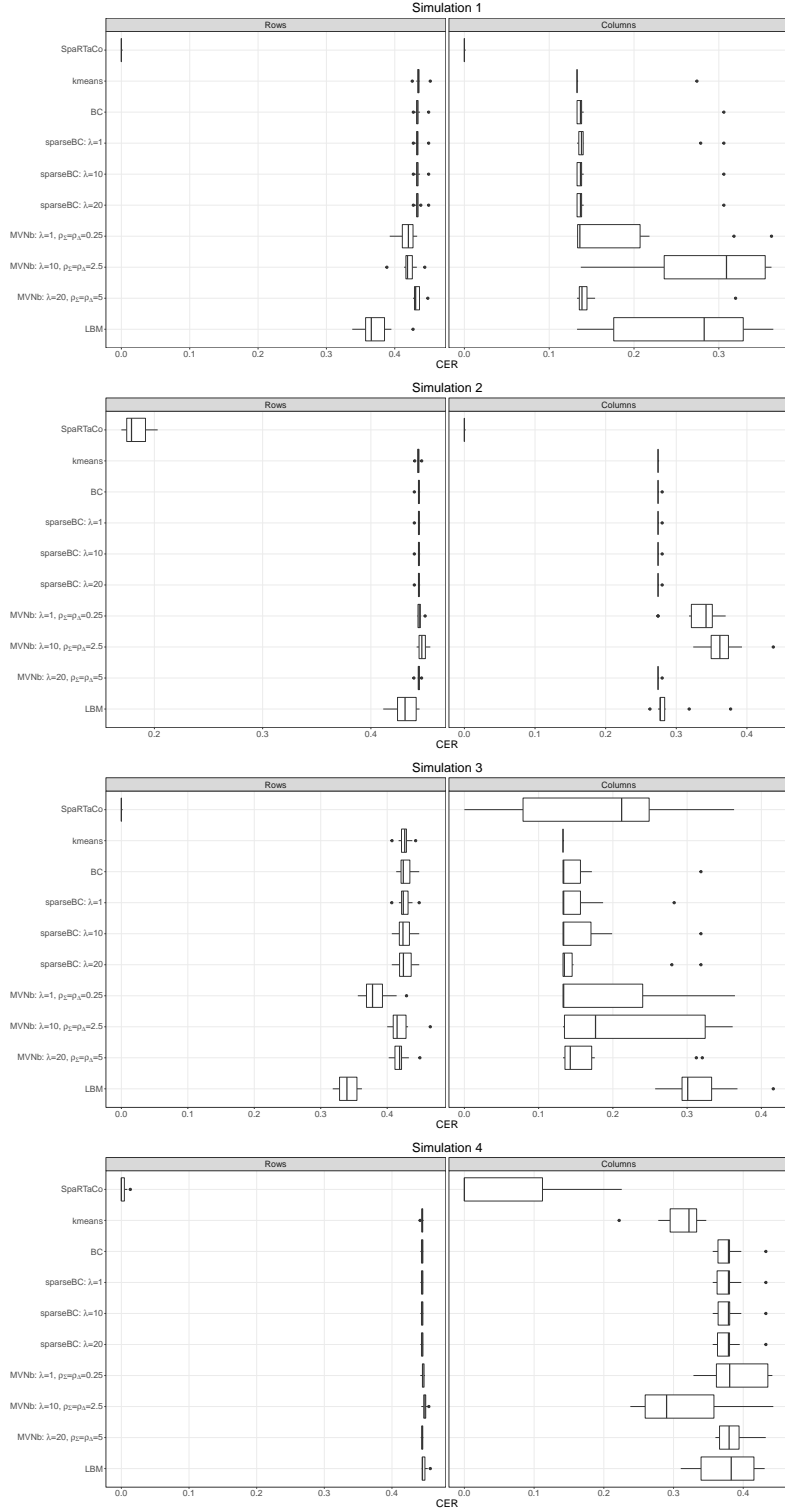


Figure 5: Results from Simulations 1-4. For each simulation we generated 10 datasets, and we applied the co-clustering models listed in Section 4.2. Every figure gives the boxplots of the CER obtained on the rows and on the columns.

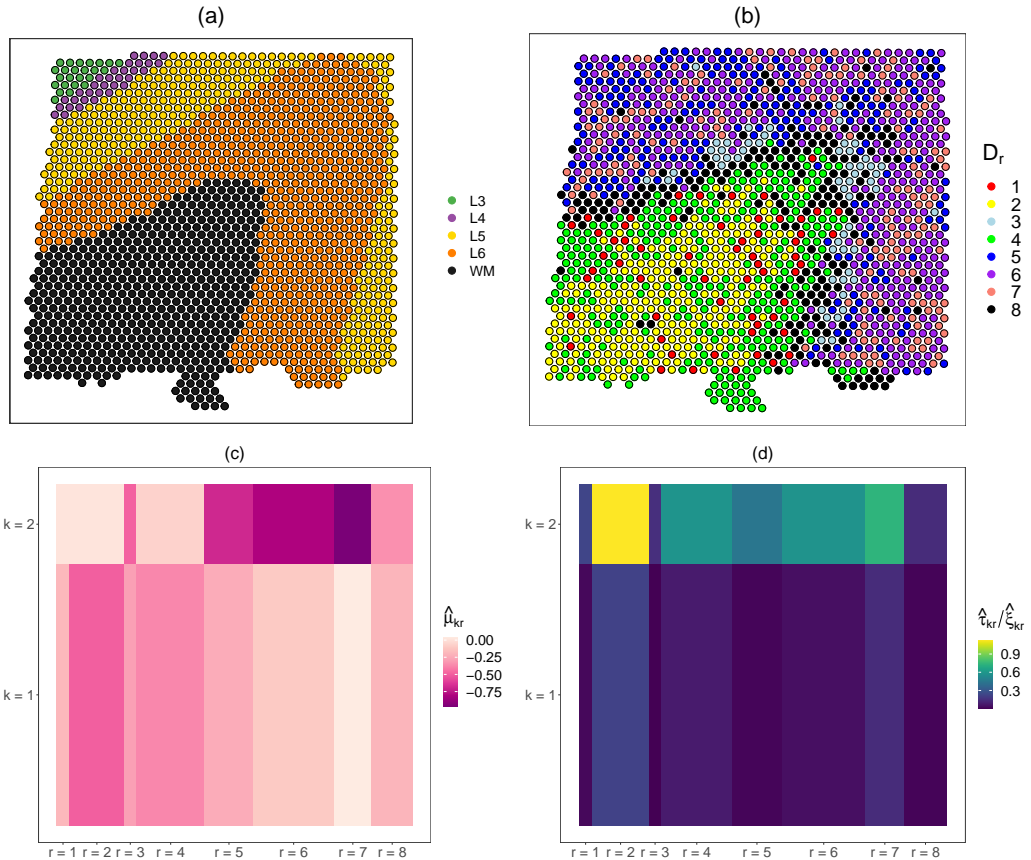


Figure 6: Results on the human dorsolateral pre-frontal cortex data. The first row displays the region of 1,585 spots colored according to the biological layers (a) and to the estimated clusters returned by SPARTACo(b). Panels (c) and (d) represent the data matrix tessellated into the 16 discovered blocks. Both the genes and the spots are reordered based on the estimated clusters for visualization purposes. The graphs are colored according to the estimated mean $\hat{\mu}_{kr}$ (c) and to the estimated spatial signal-to-noise ratio $\hat{\tau}_{kr}/\hat{\xi}_{kr}$ (d).

Co-clustering of Spatially Resolved Transcriptomic Data

Supplementary Material

A. Sottosanti¹ and D. Risso¹

¹University of Padova, Department of Statistical Sciences,
via Cesare Battisti 241-243, Padova, Italy

October 12, 2021

Address for correspondence: andrea.sottosanti@unipd.it

1 Derivation of the ICL for SpaRTaCo

Let m be the current model, and K and R be the number of row and column clusters. The *integrated classification likelihood* (Biernacki *and others*, 2000) is defined as

$$\begin{aligned} p(\mathbf{X}, \mathbf{Z}, \mathbf{W}; m, K, R) &= p(\mathbf{X}|\mathbf{Z}, \mathbf{W}; m, K, R)p(\mathbf{Z}, \mathbf{W}; m, K, R) \\ &= p(\mathbf{X}|\mathbf{Z}, \mathbf{W}; m, K, R)p(\mathbf{Z}; m, K)p(\mathbf{W}; m, R). \end{aligned} \tag{1}$$

According to Biernacki *and others* (2000), the conditional distribution of \mathbf{X} given the clustering labels can be approximated as

$$\log p(\mathbf{X}|\mathbf{Z}, \mathbf{W}; m, K, R) \approx \max_{\Theta} \log p(\mathbf{X}|\mathbf{Z}, \mathbf{W}; \Theta, m, K, R) + \frac{\lambda_{m, K, R}}{2} \log np,$$

where the first component is the classification log-likelihood evaluated in its maximum, and $\lambda_{m, K, R}$ is the number of free parameters in model m with K and R clusters. Thus, under the identifiability constraint in Section 3.1, $\lambda_{m, K, R} = 4KR + \dim(\phi)R$. The distribution of both \mathbf{Z} and \mathbf{W} is Multinomial with probabilities $1/K$ and $1/R$, respectively.

It follows that

$$\log p(\mathcal{Z}; m, K) = -n \log K, \quad \log p(\mathcal{W}; m, R) = -p \log R.$$

Finally, taking the logarithm of (1) and replacing \mathcal{Z} and \mathcal{W} with their estimates $\hat{\mathcal{Z}}$ and $\hat{\mathcal{W}}$, we obtain the ICL.

2 Spatial covariance functions

The following isotropic spatial covariance functions have been employed to generate the spatial experiments proposed in Section 4 of the manuscript:

$$k_1^{\text{true}}(d; \boldsymbol{\phi}_1^{\text{true}} = \{\theta_E\}) = \exp\left(-\frac{d}{\theta_E}\right), \quad k_2^{\text{true}}(d; \boldsymbol{\phi}_2^{\text{true}} = \{\theta_R, \alpha_R\}) = \left(1 + \frac{d^2}{2\alpha_R\theta_R^2}\right)^{-\alpha_R}.$$

$$k_3^{\text{true}}(d; \boldsymbol{\phi}_2^{\text{true}} = \{\theta_G\}) = \exp\left(-\frac{d^2}{2\theta_G^2}\right),$$

$k_1^{\text{true}}(\cdot; \theta_E)$ is the *Exponential* kernel with scale θ_E , $k_2^{\text{true}}(\cdot; \{\theta_R, \alpha_R\})$ the *Rational Quadratic* kernel with non-negative parameters (α_R, θ_R) , and $k_3^{\text{true}}(\cdot; \theta_G)$ is the *Gaussian* kernel (known also as *Squared Exponential*) with *characteristic length-scale* θ_G .

3 Covariance matrices of the genes

Here, we describe the main characteristics of the simulated covariance matrices simulated as in Formula (4.7) of the manuscript. The degrees of freedom of a Wishart distribution have to be at least equal to the matrix dimension, that is 200. Both the scales and the degrees of freedom are selected in such a way that the values in $\boldsymbol{\Sigma}_k^{\text{true}}$ have the same order of magnitude of c^{true} . For example, using the illustrated setup, the elements on the diagonals of $\boldsymbol{\Sigma}_1^{\text{true}}$ and $\boldsymbol{\Sigma}_2^{\text{true}}$ have expected values 6.3 and 11.5, respectively. The top line of Figure 1 displays the histogram of the diagonal values of a single realization of $\boldsymbol{\Sigma}_k^{\text{true}}$, for $k = 1, 2, 3$. The values are globally comparable across the three simulations. The bottom line of Figure 1 illustrates the elements out of the diagonal of $\boldsymbol{\Sigma}_k^{\text{true}}$. The difference between the first and the two other matrices is graphically visible: $\boldsymbol{\Sigma}_1^{\text{true}}$ is in fact the one with the smallest covariance values. The second and the third appear similar: in $\boldsymbol{\Sigma}_2^{\text{true}}$, the elements out of the diagonal are in the range $(-3.2, 3.1)$, while in $\boldsymbol{\Sigma}_3$ they are in the range $(-3.88, 3.81)$.

4 Additional figures

This section gives some additional figures from Section 2, 4 and 5 of the manuscript.

Section 2

Figure 2 gives a representation of the relations across co-clustering models described in Section 2.2 of the manuscript.

Section 4

Figure 3 shows the results of the model selection performed in Section 4.2 using the ICL criterion. According to the notation defined in Section 4.6 of the manuscript, Figure 4 shows a single realization of \mathbf{X}_s , \mathbf{X}_b and \mathbf{X} using $\lambda_s = \lambda_b = \sqrt{0.5}$. Last, Figure 5 shows the results of the model selection performed in Section 4.7.

Section 5

Figure 6 displays the genes ordered according to the deviance criterion proposed by Townes *and others* (2019). The red line denotes the number of genes selected for our analysis ($n = 1000$), the blue line is the “ideal” number of genes that should be used ($n = 200$), based on where the deviance curve has a significant change in the decay. Figure 7 and 8 display the conditional distributions of $\sigma_{kr,i}^2$ given the data and the parameter estimates.

References

BIERNACKI, CHRISTOPHE, CELEUX, GILLES AND GOVAERT, GÉRARD. (2000). Assessing a mixture model for clustering with the integrated completed likelihood. *IEEE transactions on pattern analysis and machine intelligence* **22**(7), 719–725.

TOWNES, F WILLIAM, HICKS, STEPHANIE C, ARYEE, MARTIN J AND IRIZARRY, RAFAEL A. (2019). Feature selection and dimension reduction for single-cell rna-seq based on a multinomial model. *Genome biology* **20**(1), 1–16.

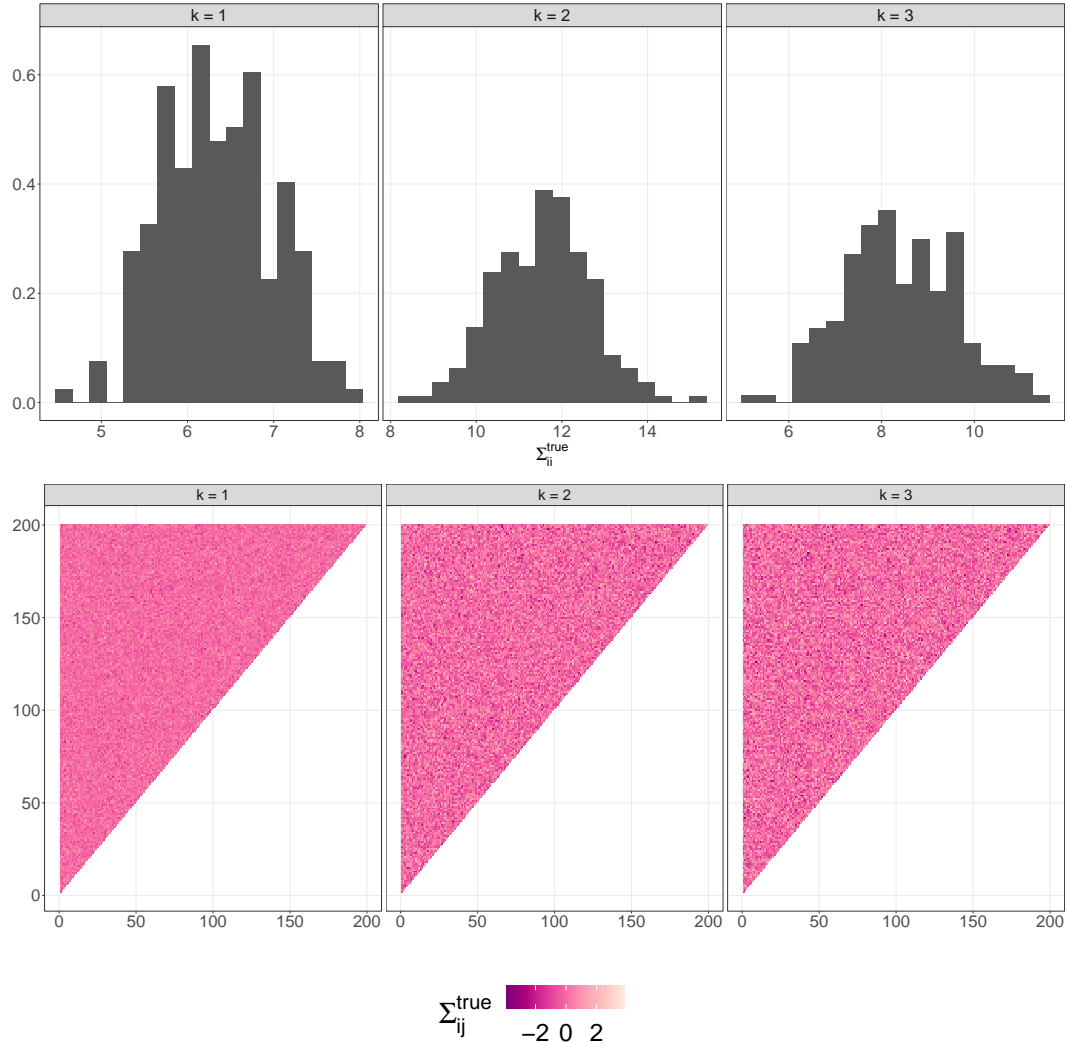


Figure 1: Plot of the row covariance matrices used in Section 2.3 of the manuscript. The top line displays the histogram of the diagonal values of Σ_k^{true} , the bottom line displays the upper triangular matrix of Σ_k^{true} , for $k = 1, 2, 3$.

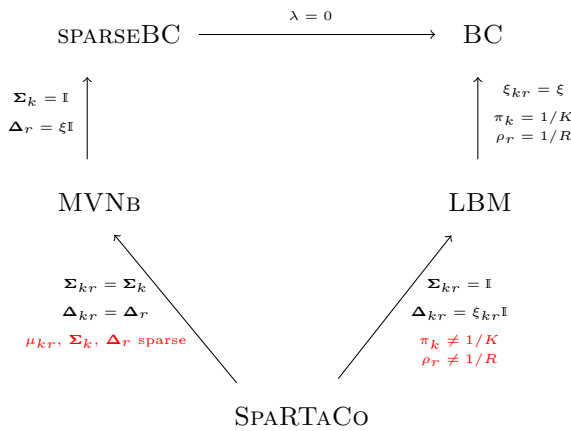


Figure 2: Map of the co-clustering models described in Section 2.2 of the manuscript. An arrow from model A to model B means that B is a special case of A. Details of how to pass from model A to model B are written in black. A red label denotes a difference between two models A and B which does not make B a special case of A.

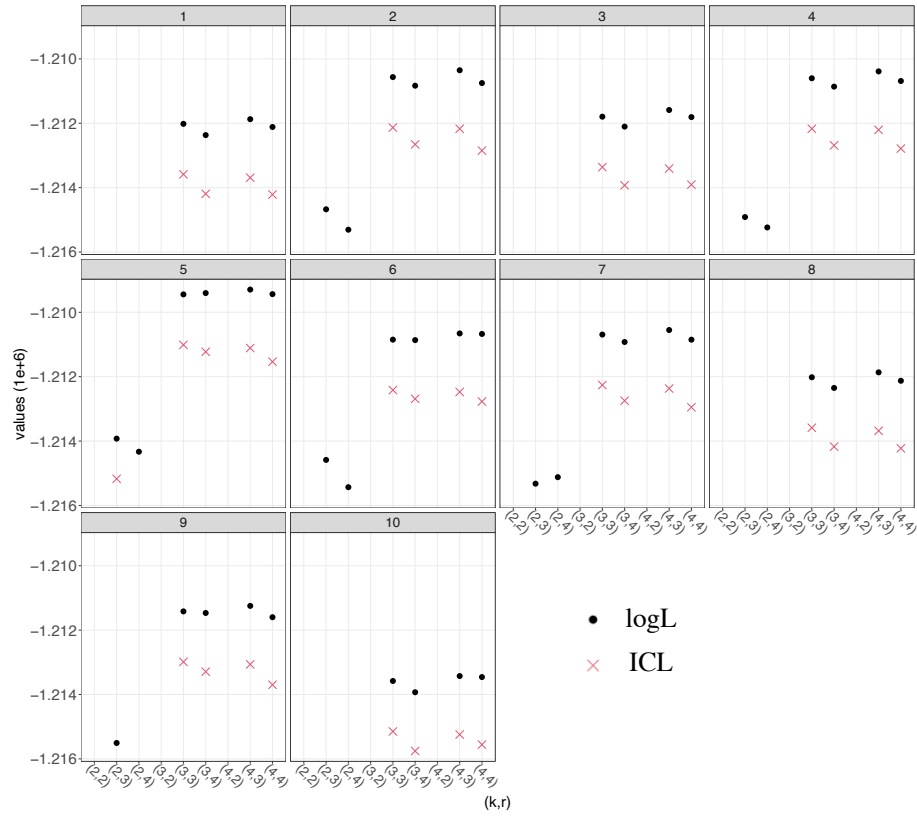


Figure 3: Results of model selection from Scenario 1. The graphs give the log-likelihood and the ICL values obtained from different configurations of SPARTACO on each of the 10 replicates of the experiment. We truncate on purpose the extremes of the y-axis to show only the models with the largest values of log-likelihood and ICL.

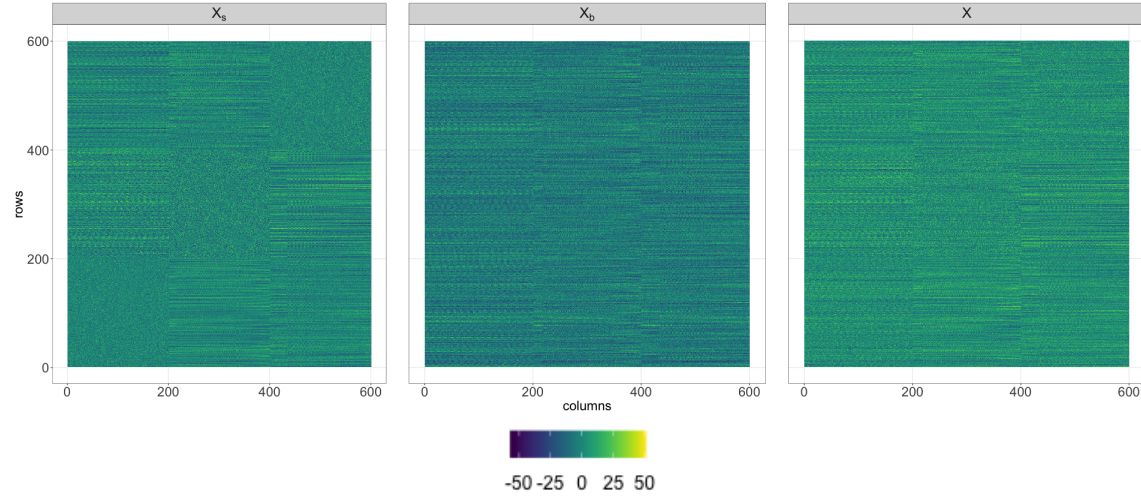


Figure 4: Simulation experiment 4. The matrices \mathbf{X}_s , \mathbf{X}_b and \mathbf{X} appear from the left to the right, using $\lambda_s = \lambda_b = \sqrt{0.5}$.

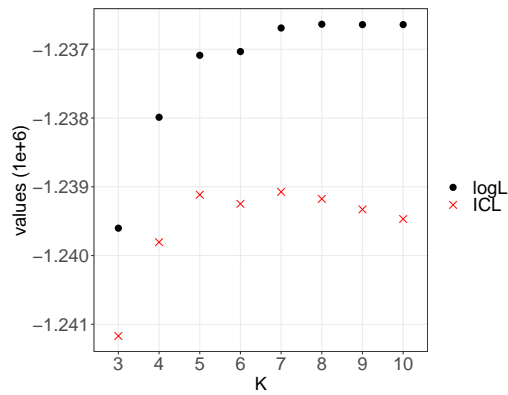


Figure 5: Model selection in Simulation 5. According to the ICL, the best model is the one with $K = 7$ row clusters. The number of column clusters is fixed to $R = 3$.

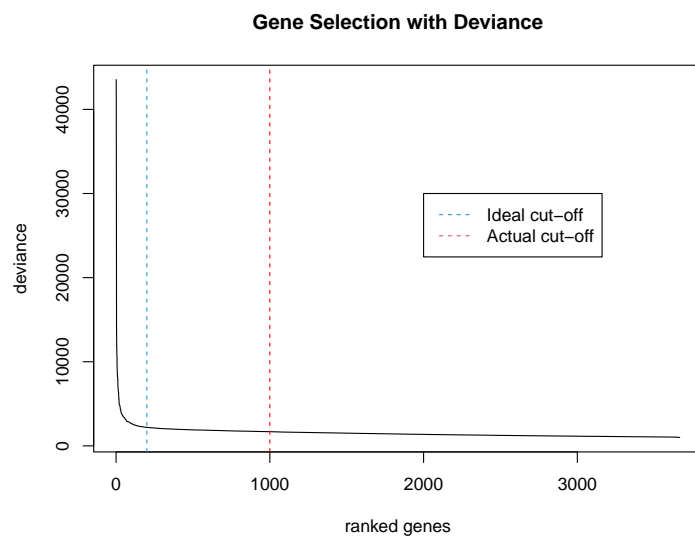


Figure 6: Graph of the genes sorted in decreasing order according to the deviance value. High deviance value are associated to informative genes. Even if from a graphical evaluation the ideal number of genes is around 200, we included in the analysis the 1,000 genes with the largest deviance.

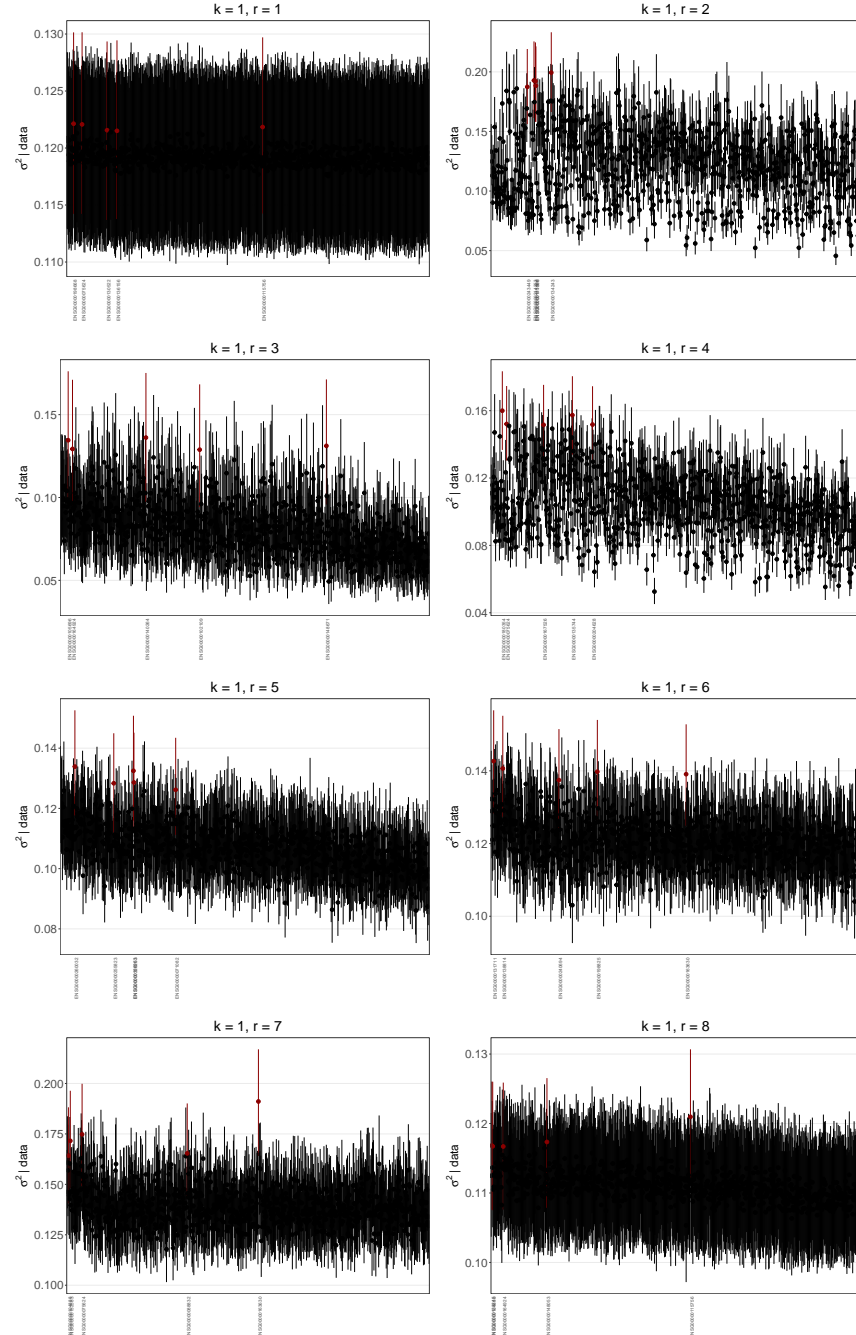


Figure 7: Distribution of $\sigma_{1r,i}^2|data$, where data denotes both the input data and the estimated quantities. The dots denote the expected values and the error bars denote the 95% credible intervals. For each block, the image colours the five genes with the largest expectation in red.

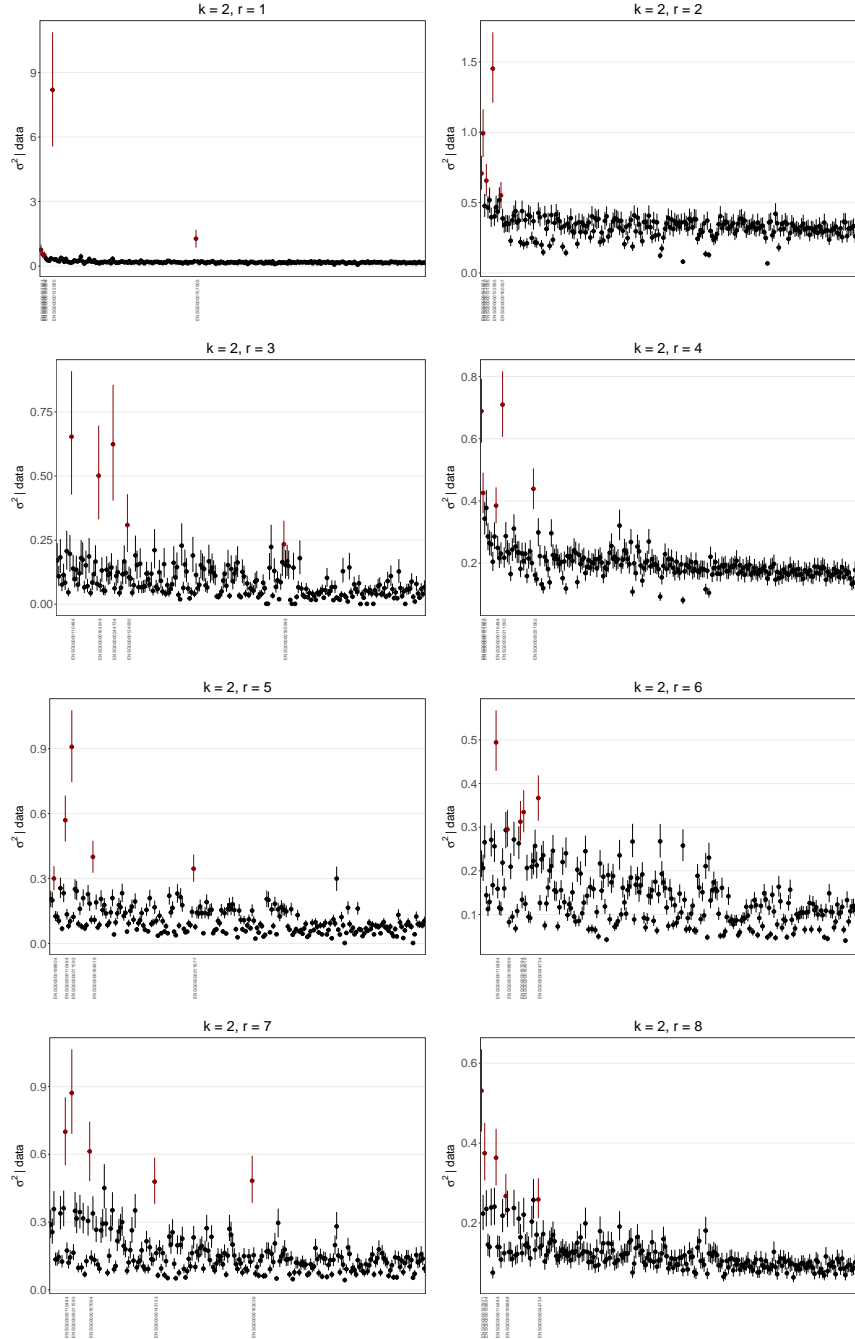


Figure 8: Distribution of $\sigma_{2r,i}^2|data$, where “data” stands for both the input data and the estimated quantities. The dots denote the expected values and the error bars are the 95% credible intervals. For each block, the image colours the five genes with the largest expectation in red.